Direct lithium extraction from natural brines with co-valorization of boron, magnesium and sodium by combining solvent extraction and electrodialysis operations

Abdoul Fattah Kiemde, César H Díaz Nieto, Jérôme Marin, Victoria Flexer, Alexandre Chagnes

Direct lithium extraction from natural brines with co-valorization of boron, magnesium and sodium by combining solvent extraction and electrodialysis operations

Abdoul Fattah Kiemde[a], Cesar H. Díaz Nieto[b], Jérôme Marin[a], Victoria Flexer[b]*, Alexandre Chagnes[a]*

[a] *Université de Lorraine, CNRS, GeoRessources, F- 54000 Nancy, France.*

[b] *CIDMEJu, CONICET - Universidad Nacional de Jujuy, Jujuy, Argentina.*

Abstract

Continental brines are the main source of lithium which could significantly contribute to meet lithium demand for electric mobility. Traditionally, lithium production from brines generates huge amount of solid waste encompassing the other brines components including boron, sodium, potassium, magnesium and calcium. From a circular economy perspective, these brine constituents should be co-valorized with lithium. This paper focuses on a novel approach to directly extract lithium from continental brine by combining solvent extraction with a three-stage electrodialysis process to produce battery-grade lithium carbonate while also co-valorizing other brine components such as boron, magnesium and sodium. Extraction solvent containing 2 mol L^{-1} 2-butyloctan-1-ol diluted in kerosene exhibited 90% extraction efficiency of boron at phase volume ratio O/A=4, 25 °C and pH=7.5. Then, the boron-loaded extraction solvent was fully stripped by 0.1 mol L^{-1} sodium hydroxide at phase volume ratio O/A=4 and 25 °C. This highly efficient and selective extraction solvent allowed to produce high-grade borax ($Na_2B_4O_7 \bullet 2H_2O$, purity=99%) by crystallization. Solvent extraction of boron was successfully implemented in a three-stage process combining electrodialysis and precipitation operations leading to the production of magnesium hydroxide ($Mg(OH)_2$, purity=71.2%), sodium carbonate (Na_2CO_3, purity=99.99%) and battery-grade lithium carbonate (Li_2CO_3, purity=99.9%). Most importantly, combining solvent extraction of boron and electrodialysis contributed to the reduction of the energy consumption by 17%. At the end of the process, the total dissolved solid (TDS) of the brine was decreased by 99.8%. This lower salinity brine can be recycled in the process and employed for farming.

1. Introduction

Lithium is a vital metal for energy transition given that it is mainly employed for manufacturing lithium-ion batteries for electric vehicles [1]. The increasing demand of electric vehicles will be responsible for huge production of lithium in the next decades [2]. Unlike many metals which are solely produced from hard-rock ores, lithium is extracted from both hard-rock ores and brines. Lithium resources from brines are about 75% of the global resources, that makes brines essential resources to ensure lithium production in the long term [3]. Continental brines as those from the salar de Hombre Muerto, salar de Atacama and salar de Uyuni in the *Lithium Triangle*, *i.e.* Argentina, Bolivia and Chile, contain significant amount of lithium as well as sodium, potassium, boron, magnesium, calcium, sulfate and chloride [4]. Lithium extraction from those brines is therefore intricate due to the high salinity (170−330 g salts L^{-1}) [4], and the presence of numerous components previously mentioned. In fact, several operations are required to remove the other brine constituents before lithium processing in order to produce high purity lithium salts.

Currently, lithium-brines facilities operate on conventional process relying on solar evaporation and chemical precipitation steps [5]. Lithium extraction by these traditional processes is accompanied with the production of other salts including gypsum ($CaSO_4 \bullet 2H_2O$), sylvinite ($NaCl \bullet KCl$), carnallite ($KCl \bullet MgCl_2 \bullet 6H_2O$), lithium carnallite ($LiCl \bullet MgCl_2 \bullet 6H_2O$), bishoffite ($MgCl_2 \bullet 6H_2O$) and borates ([6],[7]). In many facilities, these salts are not co-valorized and are stored in landfills with potential environmental risks [8]. In addition, this conventional process is responsible for huge amount of water loss during solar evaporation [8]. To overcome these issues, new technologies have been developed to bypass solar evaporation, ensure sustainable lithium production while producing lithium efficiently. Liquid-liquid extraction, solid-liquid extraction and membrane technologies were investigated at lab and demonstration scales [9]. Most of these technology do not co-valorize the other constituents even though they could be co-valorized for economic purpose. Indeed, magnesium and potassium are used as fertilizers, acidic waste neutralizers and in flame-retardant composite materials ([10], [11], [12], [13]). Sodium is used for manufacturing soda-lime glasses, fiber glasses, papers and detergents [14]. Calcium is a raw material used in glass and ceramic industries [15]. Boron is employed in glass, ceramic agriculture, detergent and nuclear industries [16]. Therefore, magnesium, calcium, sodium, potassium and boron should be co-valorized along lithium production in the next generations of lithium plants.

Nowadays, electrodialysis appears as a relevant technology in hydrometallurgy that could be employed in many applications including direct lithium extraction from brines ([9], [17], [18], [19]). In this context, we proposed a three-stage electrodialysis process allowing selective extraction of lithium and co-valorization of magnesium, calcium and sodium ([14], [20], [21]). Magnesium and calcium were recovered as magnesium hydroxide ($Mg(OH)_2$) and calcium hydroxide ($Ca(OH)_2$), respectively, while sodium was extracted as sodium carbonate. In the last stage, lithium was produced as lithium carbonate. However, boron was still not co-valorized and instead precipitated with magnesium and calcium as magnesium and calcium borates, respectively, reducing the purity of the obtained $Mg(OH)_2$ and $Ca(OH)_2$ [22]. Furthermore, less than 25 mg L^{-1} boron is required to ensure battery-grade lithium salts production [23]. Therefore, boron extraction could improve the performance of the aforementioned electrodialysis process and meet the demand of boron-intensive industries, including glass, ceramics, fertilizers, detergents and nuclear applications.

Solvent extraction of boron from brines is a mature technique already implemented in lithium facilities [24]. Extraction solvent composed of 2-butyloctan-1-ol showed remarkable extraction efficiency and selectivity for boron [25]. In addition, compare to the conventional alcohol-based extraction solvents [24], 2-butyloctan-1-ol provides less solubility in brines contributing to reduce both effluents treatment and operating costs. Therefore, this work delved into a combination of solvent extraction and electrodialysis operations in order to co-valorize boron, discard the other brine components and produce battery-grade lithium carbonate.

In the present work, boron was extracted by 2 mol L^{-1} 2-butyloctan-1-ol diluted in kerosene at phase volume ratio O/A=4, pH=7.5 and 25 °C. The boron-loaded extraction solvent was then striped by 0.1 mol L^{-1} sodium hydroxide solution. The resulting stripping solution was crystallized at 20 °C to produce boron in the form of borax. Subsequently, the boron-depleted brine was processed through electrodialysis to successively produce high-purity magnesium hydroxide, sodium carbonate, and, most importantly, battery-grade lithium carbonate salts.

2. Materials and methods

2.1. Chemicals and brine

2-butyloctan-1-ol (purity=95%), kerosene (Low odour) and m-xylene (purity=99%) were provided by Sigma-Aldrich (France). Nitric acid (HNO_3, purity=65%, Sigma-Aldrich), sodium carbonate (Na_2CO_3, purity=99.5%, Cicarelli), sodium bicarbonate ($NaHCO_3$, purity=99.7%, Cicarelli), lithium carbonate (Li_2CO_3, purity=99.99%, Sales de Jujuy), hydrochloric acid (HCl, purity=36.5%, Sigma-Aldrich) and sodium hydroxide (NaOH, purity=99%, VWR) were used as received to conduct experiment tests. A natural brine from north-western Argentina, in the Lithium Triangle (de-identified site) directly pumped from underground deposits was used as received. Composition of this brine is listed in Table 1.

Table 1: Composition, total dissolved solid (TDS) and pH of the natural brine.

Concentrations (mg L^{-1})								pH	TDS ($g\ L^{-1}$)
B	K^+	Li^+	Mg^{2+}	Na^+	Ca^{2+}	Cl^-	SO_4^{2-}		
508	6,812	578	2,316	91,733	119	176,145	14,130	7.5	305

2.2. Solvent extraction of boron

Boron extraction and stripping experiments were performed under the following extraction and stripping conditions: 2 mol L^{-1} 2-butyloctan-1-ol diluted in kerosene, the brine pH was not modified (pH=7.5), O/A=4 and 25 °C for the extraction step; and 0.1 mol L^{-1} sodium hydroxide, O/A=4 and 25 °C for the stripping step. Therefore, 4 L of the extraction solvent were mixed with 1 L of native brine . Both extraction and stripping operations were performed by mixing the organic and aqueous phases in 10 L-glass vessels using two propellers composed of four blades each. The first propeller was fixed in the middle of the aqueous phase and the second propeller was in the middle of the organic phase so that the steady state was reached after 5 min stirring at 216 rpm (see Figure A. 1 in Supplementary Information and the data of extraction and stripping equilibria tests in Table A. 1 Supplementary Information). After extraction or stripping, the organic-aqueous phases mixtures were let to settle for

5 min and the 2 phases were separated. The resulting boron-loaded organic phase was employed for the stripping test. Eight batch boron extractions were performed, before the boron-depleted brine was further processed by electrodialysis. After boron stripping, the boron-free organic phase was used to perform the next extraction experiment.

The extraction and stripping efficiencies of boron (E_B(%) and SE_B(%), respectively) were calculated as follows:

$$E_B(\%) = \frac{[B]_0 - [B]}{[B]_0} \times 100 \quad (1)$$

$$SE_B(\%) = \frac{[B]'}{[B]_0 - [B]} \times 100 \quad (2)$$

where $[B]_0$ and $[B]$ are the concentrations of boron in the brine before boron extraction and after boron extraction, respectively. $[B]'$ is boron concentration in the stripping solution at equilibrium.

The stripping solution was concentrated by evaporation with a rotary evaporator (VWR, France, heating at 45 °C under vacuum ca.10 mbar). In a first experiment, water was fully removed from the stripping solution. In a second experiment, water was removed until reaching a supersaturated borax solution. All solids obtained were washed with pure ethanol (VWR, France) and dried in oven at 100 °C for 30 min.

2.3. Electrodialysis operations

The non-pretreated brine, *i.e.* brine without boron extraction, and the boron-depleted brine, *i.e.* brine after boron extraction, were processed by electrodialysis in three stages (Figure A. 2 in Supporting Information). The electrodialysis cells were composed of three compartments, i.e. anodic, middle and cathodic compartments. In stage I, calcium and magnesium were removed in the cathodic compartment. Then, the outlet of the cathodic compartment of stage I fed the middle compartment of stage II where sodium was recovered as sodium carbonate. Finally, the outlet of the middle compartment of stage II fed into the middle compartment of stage III, where lithium was converted into lithium carbonate. The electrodialysis experiments were performed in batch mode at room temperature 22±2 °C. The cells were made of acrylic frames and designed as reported in literature ([26], [27]). Cation exchange membrane (CEM) (CMI-7000S, Membrane International Inc., USA) or anion exchange membrane (AEM) (AMI-7001CR, Membrane International Inc., USA) were employed to separate each compartment of the cells. Table A. 2 in Supplementary Information gave the membrane specifications. The anodic, middle and cathodic compartments were connected each to a glass bottle. The aqueous solution in each compartment was constantly recirculated through the cell compartments by means of a peristaltic pump (flow rate=18 L h^{-1}). Titanium (Ti) mesh electrode coated with an iridium-based mixed metal oxide (IrO_2/TiO_2; 65/35%, Magneto Special Anodes) was used as

anode. This anode contained a perpendicular current collector. The cathode was a stainless-steel wire mesh with a stainless-steel current collector. Distance of 23 mm was kept between the electrodes. In order to avoid direct contact between the electrodes and the membranes, , two plastic meshes were placed between the surface of the electrodes and the membranes. Experiments were run in galvanostatic mode by means of a DC/CC regulated power supply. The projected geometric surface of the membrane in contact with the solutions were employed to calculate the current densities. For specific membrane and electrode arrangement in each Stage, see Figure A. 2.

In the stage I, the volume of each compartment and the surface area of the membrane were contacted with the solutions were 200 mL and 0.01 m^2, respectively. The anodic compartment and the middle compartments were connected each to glass bottles containing 0.05 mol L^{-1} nitric acid (HNO_3) and 0.01 mol L^{-1} hydrochloric acid (HCl), respectively. While the cathodic compartment was connected to a glass bottle that was employed as a decanter and contained, alternatively the non-pretreated brine or the boron-depleted brine. The volume of anolyte, catholyte or brine was 1 L. This electrodialysis stage lasted 5 hours. The recovered precipitates were centrifuged at 3,200 rpm for 15 min. The electrodialysis was conducted at an applied current density of 215 A m^{-2} during 5 hours.

In stage II, the cathodic and middle compartments were connected each to a glass bottle containing 250 mL of 0.1 mol L^{-1} sodium bicarbonate (pH=9.4) and 500 mL of stage I outlet, respectively. High volume ratio between the solution in the middle compartment and the catholyte should allow for the concentration of cations in the catholyte. The electro-membrane experiments were performed up to 30 V, since high drop of ion concentration in the middle compartment increases the cell voltage[14]. The electrodialysis experiments were carried out at 150 A m^{-2}.

Three consecutive electrodialysis experiments were carried out in batch in Stage II with the non-pretreated brine or the boron-depleted brine. Each experiment was stopped when the pH of catholyte reached about 14, to preserve the membranes. The cations-loaded catholyte was transferred to a glass bottle where CO_2 was bubbled until pH=7.7−8 in order to precipitate sodium as $NaHCO_3$. The precipitate was recovered by vacuum filtration. After filtration, the mixture of sodium depleted catholyte (supernatant) and filtrate from solid wash was returned to the to perform the subsequent electrodialysis experiment.

In stage III, the cathodic and middle compartments were each connected to a glass bottle containing 150 mL of 0.1 mol L^{-1} lithium carbonate (Li_2CO_3) and 200 mL of the sodium-depleted catholyte obtained after the final precipitation in stage II , respectively (see Figure A.2). Unfortunately, the low volume ratio between the solution in the middle compartment and the catholyte (1.3), along with water migration from the middle compartment to both the catholyte and anolyte, limited cation concentration in the catholyte. The electrodialysis experiment was performed for 11 hours until the voltage reached 30 V. The catholyte was then transferred into a glass bottle for CO_2 bubbling for 1h30 min until the pH reached 9.4. No precipitate was observed as the solubility of Li_2CO_3 was not reached in the catholyte due to the low lithium concentration. Therefore, Li_2CO_3 was crystallized by evaporation at 90 °C. Evaporation was stopped when the catholyte volume was reduced by four.

All recovered solids were washed with deionized water, and dried in a laboratory oven at 100 °C for 24 hours.

In stages II and III, the total volume for each compartment and the surface area of the membrane in contact with the solutions were 100 mL and 0.005 m^2, respectively. Additionally, the anodic and middle compartments were separated by an anion exchange membrane (AEM), and the middle and cathodic compartments were separated by a cation exchange membrane (CEM). The electro-membrane experiments in stages II and III were focused on the transfer of cations from the middle to the cathodic compartment and anions transfer from the middle compartment to the anodic compartment. Therefore, chloride transfer into the anodic compartment responsible for chlorine gas formation at pH below 7 [28]. For safety reasons, the anodic compartment was connected to a glass bottle containing 2 L of 0.5 mol L^{-1} sodium carbonate (Na_2CO_3, pH=11.4), which buffered the solution at pH=11 and allowed to disproportionate Cl_2 into Cl^- and ClO^-[28].

- The circulated charge per liter of brine (C L^{-1}) was calculated as follows:

$$\text{Circulated Charge} = \frac{i \times t}{V} \tag{3}$$

where i (A) and t (s) are the applied constant current and the electrodialysis time, respectively. V is the volume of the brine employed for the electrodialysis experiment.

- The normalized concentration (C/C_0) referred to the ratio between the concentration of an element at time t in a given electrodialysis compartment (C) and the initial concentration (C_0) of this element in the same compartment.

- The electrochemical energy consumption per volume of treated brine (Wh L^{-1}) was calculated as follows:

$$\mathrm{E} = \int_0^{\mathrm{t}} \frac{E_{source} \times i \times dt}{V_0} \tag{4}$$

where E_{source} (V) is the voltage drop in the electrodialysis cell and V_0 (L) is the initial brine volume.

- The separation coefficient ($\mathrm{F_{M_1-M_2}}$) referred to the ratio of concentrations in the middle compartment of coexisting cations at time t divided by the ratio of the initial concentrations:

$$\mathrm{F_{M_1-M_2}} = \frac{\left(C_{M_1}/C_{M_2}\right)_{\mathrm{t}}}{\left(C_{M_1}/C_{M_2}\right)_0} \tag{5}$$

where C_{M_1} and C_{M_2} are the concentrations of cations $\mathrm{M_1}$ and $\mathrm{M_2}$, respectively. If $\mathrm{F_{M_1-Li}} > 1$ then lithium passes through the CEM preferentially.

2.4.Speciation calculations

Speciation calculations in aqueous phases were performed with the software Phreeqc ver. 3.7 [29]. Speciation diagrams were plotted with PhreePlot which is a charting and plotting extension of Phreeqc. Regarding the high salinity of the brine, the distribution of the species in the aqueous phases was performed by using Minteq.V4 databases. Non-ideality in aqueous solutions was accounted for in Phreeqc using the Pitzer model. For this purpose, the speciation model required element concentrations, pH, temperature, density and redox potential of the aqueous phase as well as the equilibrium constants or reaction enthalpies of the chemical reactions occurring in the aqueous phases. Therefore, the selected equilibrium constants and reaction enthalpies data must be reliable and consistent to provide accurate calculations. Boron speciation in the aqueous phases was calculated using the thermodynamic constants. The corresponding chemical reactions included in the databases for speciation calculations are reported in Table 2.

Table 2: Chemical reactions and thermodynamic constants used for speciation calculations of boron with Phreeqc (databases: Pitzer and Minteq.V4).

Chemical reaction	log (K)
$H_3BO_3 \rightleftarrows H_3BO_3$	0
$H_3BO_3 + H_2O \rightleftarrows B(OH)_4^- + H^+$	-9.2
$H_3BO_3 \rightleftarrows H_2BO_3^- + H^+$	-9.2
$2H_3BO_3 \rightleftarrows H_5(BO_3)_2^- + H^+$	-9.3
$3H_3BO_3 \rightleftarrows H_8(BO_3)_3^- + H^+$	-7.3
$3H_3BO_3 \rightleftarrows B_3O_3(OH)_4^- + 2H_2O + H^+$	-7.5
$4H_3BO_3 \rightleftarrows B_4O_5(OH)_4^{2-} + 3H_2O + 2H^+$	-16.1
$Ca^{2+} + H_3BO_3 + H_2O \rightleftarrows CaB(OH)_4^+ + H^+$	-7.6
$Ca^{2+} + H_3BO_3 \rightleftarrows CaH_2BO_3^+ + H^+$	-7.5
$Mg^{2+} + H_3BO_3 + H_2O \rightleftarrows MgB(OH)_4^+ + H^+$	-7.8
$Mg^{2+} + H_3BO_3 \rightleftarrows MgH_2BO_3^+ + H^+$	-7.7
$Na^+ + H_3BO_3 \rightleftarrows NaH_2BO_3 + H^+$	-9

2.5.Analyses

The aqueous solutions were sampled for chemical analyses. Magnesium and calcium concentrations were determined by complexometric titrations with EDTA (Anedra, p.a.). Eriochrome Black T (Anedra, p.a.) and Murexide (Anedra, p.a.) were used as complexometric indicators to determine the endpoint. Concentrations of magnesium and calcium obtained by titration were confirmed by microwave plasma-atomic emission spectrometer analyses (MP-AES model 4210, Agilent, France). Concentrations of lithium, boron, potassium, magnesium, calcium and sodium were determined at 670.784 nm, 249.677 nm, 766.491 nm, 518.360 nm, 393.366 nm and 568.820 nm,

respectively. Concentrations of Cl^- and SO_4^{2-} were determined by chromatographic analyses (Dionex ICS 900 ™ IonPac™ AS22). The pH was determined with a pH-meter (Hanna), and confirmed by universal pH test paper strips. The repeatability of the experiments was assessed by repeating them twice. The relative error remained below 4%.

All the solids were grounded before XRD analysis. The bulk mineralogy of the suspended particle matter (SPM) was determined by X-ray diffraction using a D8 Discover Bruker diffractometer with an X-ray tube emitting Cu-Kα1 radiation (λ=1.5406 Å). X-ray diffraction patterns were recorded at 40 kV and 40 mA on powder samples under ambient conditions and within a range of 2θ (2.5°−65°), a step size of 0.035°, and a 3-s collection time with a LynxEye detector. The phases were identified by using the database of the X-ray diffractometer software (EVA software).

3. Results and discussion

3.1. Boron extraction, stripping and crystallization

Eight batch boron extractions were required to recover 90% of boron from the native brine (see Table A. 3 in Supplementary Information). Analysis of the stripping solution indicated it contained 0.9 g L^{-1} boron and 2.3 g L^{-1} sodium, this latter amount corresponds to the as prepared NaOH solution. Complete water evaporation took 24h in conditions described in Materials and Methods. X-ray diffraction (XRD) analysis of the resulting solid S_1 showed that the solid is teepleite ($Na_2B(OH)_4Cl$) (Figure 1 (a)) [30]. The formation of teepleite is attributed to the presence of chloride ions in the stripping solution, which were co-extracted and co-stripped during the extraction and the stripping steps. Analysis of the stripping solution confirmed the presence of 484.4 mg L^{-1} chloride. Indeed, chloride can be co-extracted with boric acid from the brine probably as hydrochloric acid by forming hydrogen bonds with the alcohol [31].

Teepleite cannot be valorized on the market, while borax can. Therefore, the subsequent work was focused on identifying the experimental conditions to prevent teepleite formation and promote borax crystallization. In a second attempt, the stripping solution was first evaporated in the same condition as previously to reach 11.76 g L^{-1} boron, making the solution supersaturated (borax solubility in water at 20 °C is 51 g L^{-1}, which is equivalent to 5.8 g L^{-1} boron [37], [38], [39]). The resulting solution was then crystallized by cooling at 20 °C during 8 hours. The crystallization efficiency reaches 54%. XRD analysis showed that the resulting solid S_2 was a mixture of borax ($Na_2B_4O_7•10H_2O$) and tincalconite ($B_2H_5NaO_6$) (Figure 1 (b)). However, pure borax ($Na_2B_4O_7•2H_2O$, purity=99%) was obtained by drying the solid at 100 °C for 24 hours.

(a)

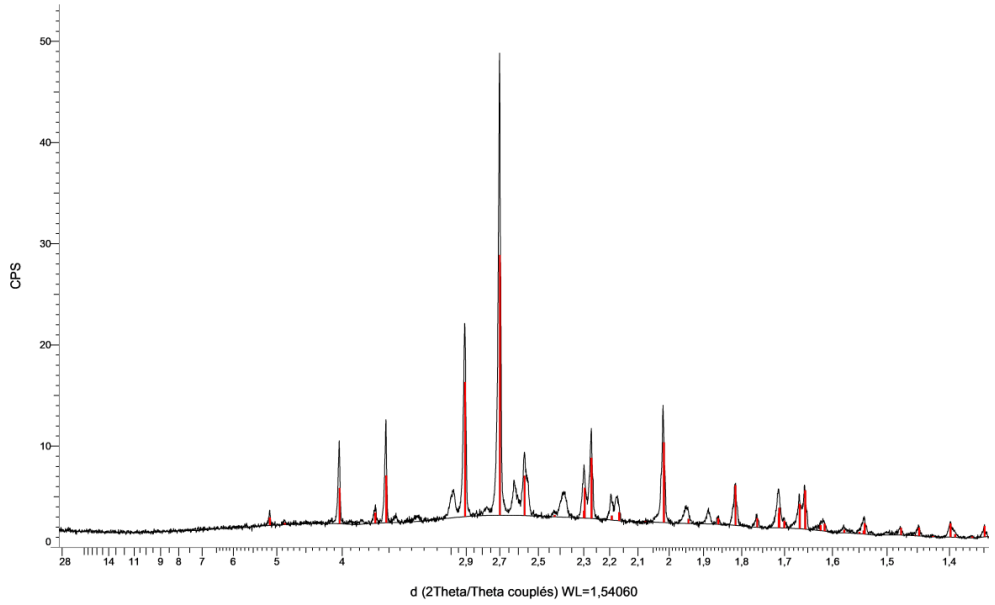

(b)

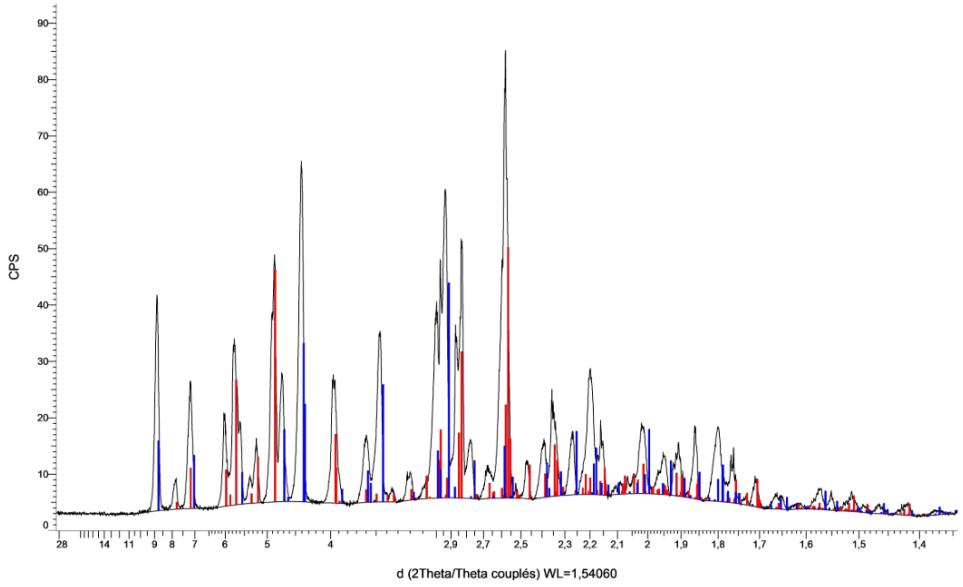

Figure 1: XRD patterns of (a) the solid S_1 (in black) and comparison with the XRD pattern of teepleite (in red) [30] and (b) of the solid S_2 (in black) and comparison with XRD patterns of borax (in red) and Tincalconite (in blue).

The brine composition before and after boron extraction is shown in Table 3. There is no significant difference in the concentrations of potassium, sodium or lithium before and after boron extraction, a good result, particularly regarding lithium considering it is the most valuable prospective product. However, a significant decrease in magnesium and calcium concentrations (11.3% and 23%, respectively) is observed. This decrease cannot be attributed to the liquid-liquid extraction of magnesium and calcium by 2-butyloctan-1-ol, as this process cannot occur under the given experimental conditions [25]. Conversely, magnesium and calcium can precipitate under alkaline conditions as magnesium hydroxide ($Mg(OH)_2$) and calcium hydroxide ($Ca(OH)_2$), respectively [28]. Hence, the slight alkalinity of the brine after boron extraction (see Table 3) may be responsible for a

precipitation of magnesium and calcium. The slight increase in brine pH is attributed to the co-extraction of hydrochloric acid, as evidenced by the decrease in chloride concentration in the brine and, as discussed above the fact that chloride anions were found in the stripping solution.

Table 3: Composition and pH of the native brine, and after boron extraction, and electrodialysis operations.

	Concentrations (mg L^{-1})								pH
	B	K^+	Li^+	Mg^{2+}	Na^+	Ca^{2+}	Cl^-	SO_4^{2-}	
Native brine	508	6,812	578	2,316	91,733	119	176,145	14,130	7.5
Brine after B extraction	**51**	6,685	546	2,055	88,802	92	155,422	12,733	8.8
Brine after Stage I electrodialysis	447	8,800	715	**0**	110,634	**0**	185,800	16,366	13.0
Brine after B extraction, Stage I electrodialysis	51	7,428	560	**0**	89,315	**0**	151,975	13,284	12.4
Brine after B extraction, Stages I and II electrodialysis	62	**0**	**7**	**0**	**251**	**0**	43	87	11.8

The brine was filtered to remove the colloidal suspension formed due to the precipitation of magnesium hydroxide [11]. After filtration, the boron-depleted brine was used to investigate magnesium and calcium removal by electrodialysis.

3.2. Magnesium and calcium removal by electrodialysis

The first electrodialysis stage was carried out with the aim to remove calcium and magnesium.

In this electrodialysis setup, in the anodic compartment, water is oxidized to oxygen (Equation 6). Simultaneously, in the cathodic compartment, water contained in the brine is reduced to hydrogen with the concurrent production of OH^- (Equation 7).

$$2H_2O \rightarrow O_2 + 4H^+ + 4e^- \quad (6)$$

$$2H_2O + 2e^- \rightarrow H_2 + 2OH^- \quad (7)$$

The pH values, current, voltage as well as boron, magnesium and calcium concentrations are reported as a function of the electrodialysis time for each type of brine (*i.e.* non-pretreated or boron-depleted brine) in Tables A. 4 and A. 5 in Supplementary Information. As shown in Figure 2, the pH of the non-pretreated brine or the boron-depleted brine increases with the circulated charge, as water reduction in the cathodic compartment generates OH^- anions (Equation 7). A similar trend is observed

for both brines, except that the pH of the boron-depleted brine increases more quickly than that of the non-pretreated brine. For instance, at 23,220 C/L, the pH of boron-depleted brine reached 12.0, while 33,250 C/L was required to reach pH=12.0 in the non-pretreated brine. Thus, the presence of boron in the brine increases the circulated charge required for the brine treatment. The pH increases observed at the early stage of the experiment are attributed to moderate precipitation phenomena, while the very slight increases in pH (almost two plateau can be observed) can be explained by significant solid precipitation. The OH^- anions produced can be consumed by both Mg^{2+}, Ca^{2+} in solution to form precipitates [20]. According to solubility product values of magnesium hydroxide ($pK_{SP,Mg(OH)2}$=11.25) and calcium hydroxide ($pK_{SP,Ca(OH)2}$=5.3) [28], $Mg(OH)_2$ is less soluble than $Ca(OH)_2$ and thus, $Mg(OH)_2$ precipitates before $Ca(OH)_2$.

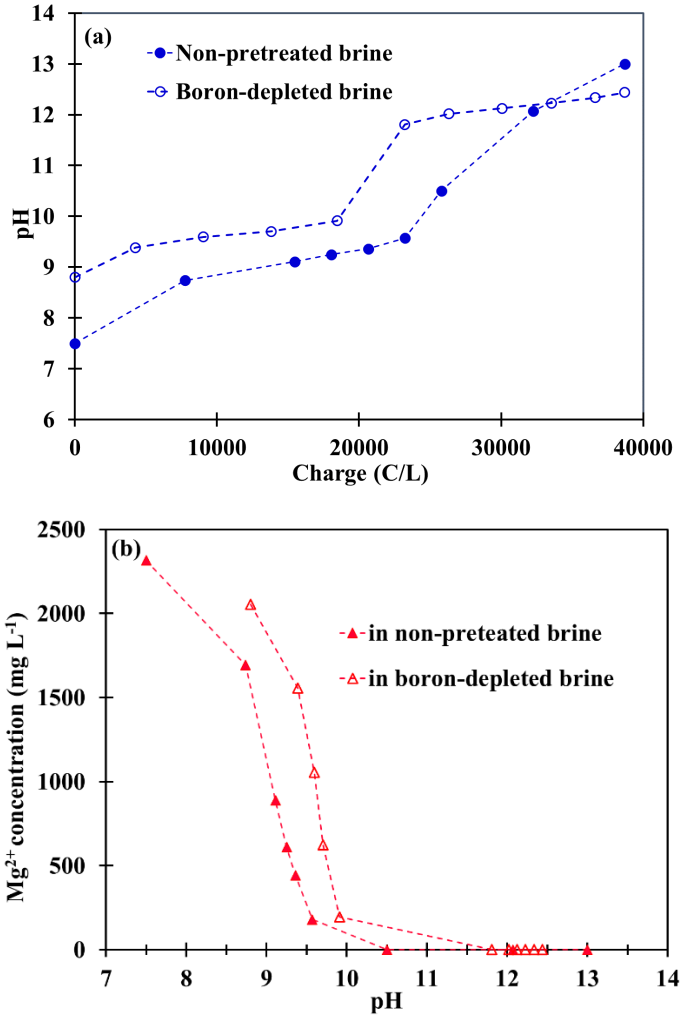

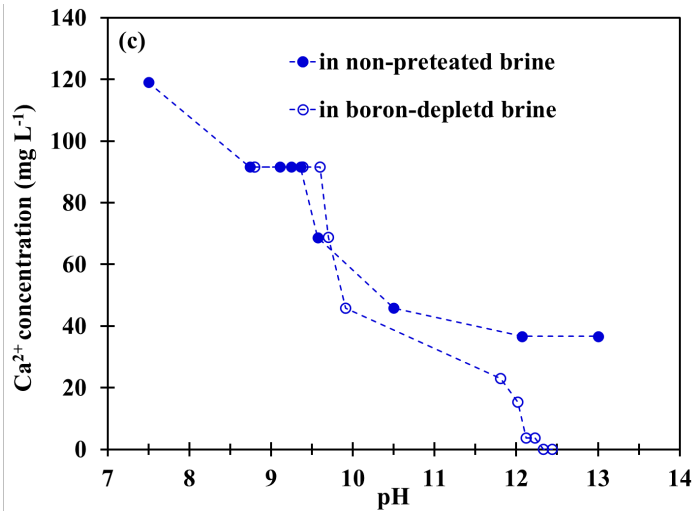

Figure 2: (a) pH of the non-pretreated brine and the boron-depleted brine as a function of the electrodialysis time; (b) Magnesium and (c) calcium concentrations in the brines as a function of the pH during the electrodialysis

Figures 2 (b) and (c) show magnesium and calcium concentrations as a function of pH in both non-pretreated brine and boron-depleted brine. A significant decrease in magnesium concentration is observed at pH 8.7−9.9 for both brines. Full precipitation of magnesium was achieved at pH 10.5 in the non-pretreated brine. Conversely, the pH had to be increased to 11.5 to totally remove magnesium by precipitation when electrodialysis experiments were conducted with the boron-depleted brine. Similar results were reported by Nieto et al. [20] for the non-pretreated brine. It might seem counterintuitive, but Figure 2 and Tables A. 4 and A. 5 clearly show that a lower amount of charge (and hence electric energy) is required to fully remove Mg^{2+} in the boron depleted brine as compared to non-pretreated brine.

The speciation diagrams (Figure 3 and 4) help to interpret the different behavior for the two brines. The The higher precipitation of magnesium at lower pH in the non-pretreated brine, compared to in the boron-depleted brine, can be attributed to the differences in concentrations of $MgOH^+$, $MgH_2BO_3^+$ and $MgB(OH)_4^+$ (Figure 3). Indeed, Mg^{2+} exist in alkaline solution as $MgOH^+$ (Equation 8) and as $MgH_2BO_3^+$ and $MgB(OH)_4^+$ in the presence of boron (Equations 10 and 12). The difference in behavior observed between the non-pretreated brine and the boron-depleted brine cannot be explained by the precipitation of $Mg(OH)_2$ from $MgOH^+$ (Equation 9) since no significant difference is observed between $MgOH^+$ speciation vs pH in the non-pretreated brine and the boron-depleted brine.

$MgH_2BO_3^+$ and $MgB(OH)_4^+$ concentrations are higher in the non-pretreated brine (Figure 3). Then, it can be inferred that magnesium precipitates at lower pH in the presence of chloride due to the formation of solids such as MgH_2BO_3Cl and $MgB(OH)_4Cl$ according to Equations (11) and (13). This assumption is supported by the presence of boron and chloride anions in the precipitate (Table A. 7 in Supplementary Information). Hence, boron favors magnesium precipitation in the non-pretreated brine but contributes to increase the circulated charge and decrease the purity of the magnesium precipitate.

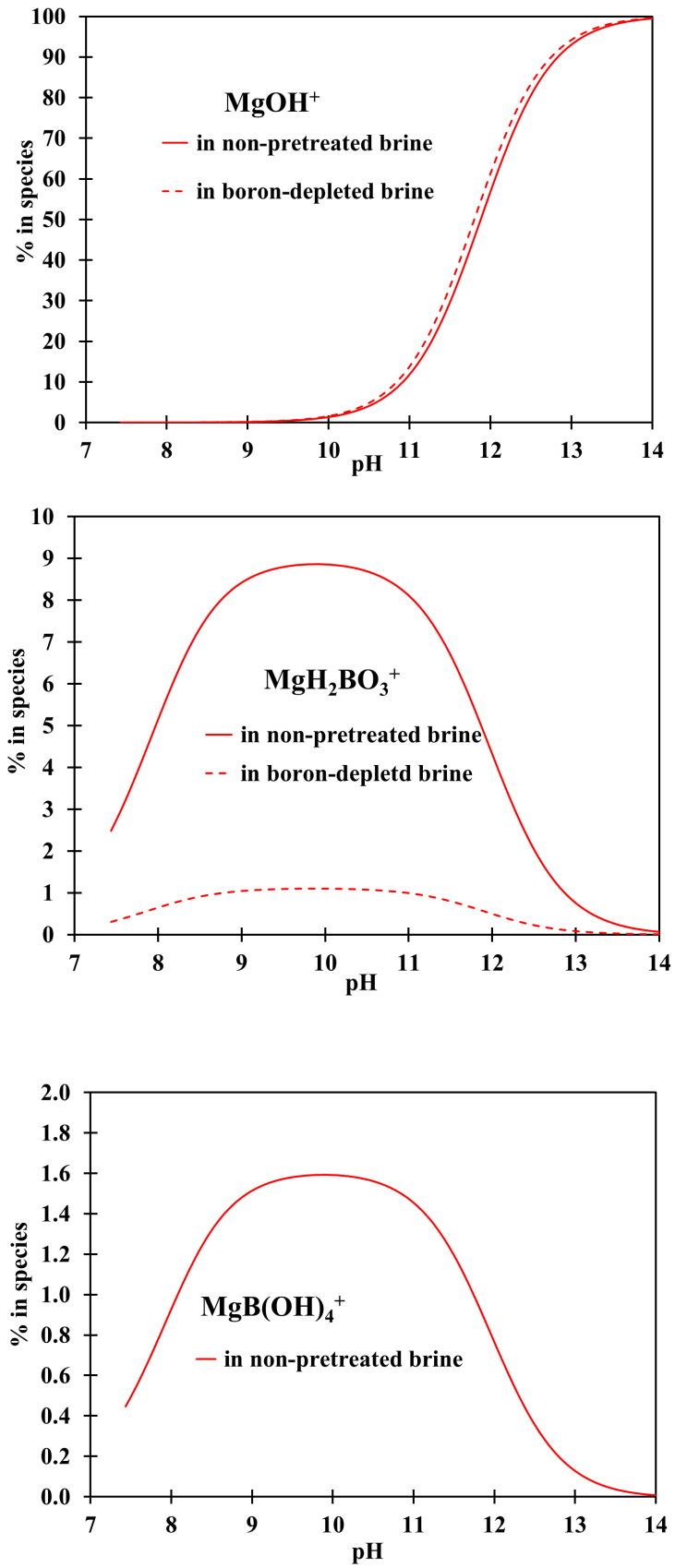

Figure 3: Magnesium speciation vs pH in the non-pretreated brine and boron-depleted brine. Only $MgOH^+$, $MgH_2BO_3^+$ and $MgB(OH)_4^+$ species were reported in these Figures.

$$Mg^{2+} + OH^{-} \rightleftarrows MgOH^{+} \quad (8)\ [28]$$

$$MgOH^{+} + OH^{-} \rightleftarrows Mg(OH)_{2(S)} \quad (9)\ [28]$$

$$Mg^{2+} + H_3BO_3 \rightleftarrows MgH_2BO_3^{+} + H^{+} \quad (10)\ [35]$$

$$MgH_2BO_3^{+} + Cl^{-} \rightleftarrows MgH_2BO_3Cl_{(S)} \quad (11)$$

$$\mathbf{Mg^{2+} + H_3BO_3 + H_2O \rightleftarrows MgB(OH)_4^{+} + H^{+}} \quad (12)\ [36], [37]$$

$$MgB(OH)_4^{+} + Cl^{-} \rightleftarrows MgB(OH)_4Cl_{(S)} \quad (13)$$

Figure 4 (b) shows that boron can contribute to decrease calcium concentration only at pH=7.5−8.8. This can be attributed to the precipitation of CaH_2BO_3Cl and $CaB(OH)_4Cl$ species (Equations 17 and 19). These species are obtained through the formation of boron-calcium species such as $CaH_2BO_3^{+}$ and $CaB(OH)_4^{+}$ species (Figure 5), which are formed according to Equations 16 and 18. The decrease of calcium concentration in the brines is also attributed to the formation of $CaOH^{+}$ (Equation 14) which precipitates as $Ca(OH)_2$ according to Equation 15. There is no influence of pH on calcium precipitation at pH=8.8−9.6 and 91.6 mg L^{-1} Ca was found in the brines (Figure 2 (c)). However, calcium precipitation is more pronounced at pH above 9.6 in the boron-depleted brine than in the non-pretreated brine. Low calcium precipitation could be explained by the formation of the highly soluble boron-calcium species CaH_2BO_3Cl and $CaB(OH)_4Cl$ in very alkaline solution. The residual calcium concentration in the non-pretreated brine (36.6 mg L^{-1}) was removed by putting the brine in contact with carbon dioxide for 24 hours. It is important to point out that boron extraction from brine could contribute to achieve selective precipitation of magnesium and calcium since magnesium hydroxide can be precipitated at pH=8.8−9.6, and calcium hydroxide can be precipitated by increasing the pH between 9.6 and 12.3.

$$Ca^{2+} + OH^{-} \rightleftarrows CaOH^{+} \quad (14)\ [28]$$

$$CaOH^{+} + OH^{-} \rightleftarrows Ca(OH)_{2(S)} \quad (15)\ [28]$$

$$Ca^{2+} + H_3BO_3 \rightleftarrows CaH_2BO_3^{+} + H^{+} \quad (16)\ [35]$$

$$CaH_2BO_3^{+} + Cl^{-} \rightleftarrows CaH_2BO_3Cl_{(S)} \quad (17)$$

$$Ca^{2+} + H_3BO_3 + H_2O \rightleftarrows CaB(OH)_4^{+} + H^{+} \quad (18)\ [36]$$

$$CaB(OH)_4^{+} + Cl^{-} \rightleftarrows CaB(OH)_4Cl_{(S)} \quad (19)$$

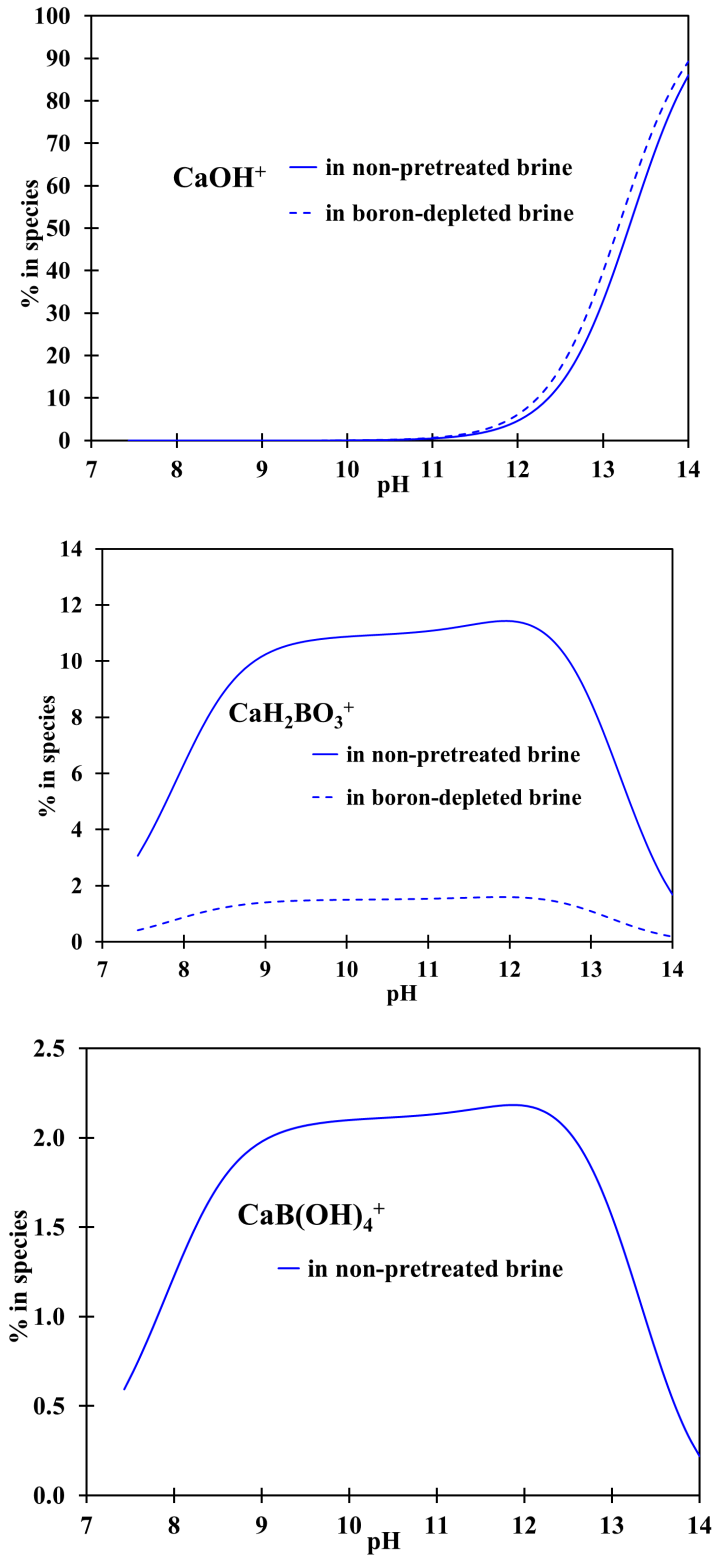

Figure 4: Ca speciation vs pH in the non-pretreated brine and the boron-depleted brine. Only $CaOH^+$, $CaH_2BO_3^+$ and $CaB(OH)_4^+$ species were reported in these Figures

Table 3 gathers boron, potassium, lithium, magnesium, sodium, calcium, chloride and sulfate concentrations in the brines before and after the stage I. The concentrations of potassium, lithium, sodium, chloride and sulfate increase slightly after the experiment for both non-pretreated brine and

boron-depleted brine. This is explained by the migration of water molecules from the cathodic compartment to the middle comportment by electroosmosis ([38], [39], [40], [41], [42]) and water reduction into OH^- and H_2 (Equation 7).

The energy consumptions were 0.062 kWh and 0.052 kWh per liter of non-pretreated brine and boron-depleted brine, respectively. This indicates that boron extraction before the electrodialysis decreases the energy consumption by 17%.

3.3. Magnesium hydroxide production

After precipitation, the solid was removed from the brines by centrifugation and filtration under vacuum. Thereafter, it was harvested and dried at 100 °C for 24 hours in oven. The weight of the solid obtained from the electrodialysis experiment carried out with the non-pretreated brine or the boron-depleted brine was higher than that calculated by considering the total amount of magnesium and calcium initially present in the brine (26.4 g vs 5.8 g for 1 liter of non-pretreated brine and 21.7 g vs 5.1 g for 1 liter of boron-depleted brine). Elemental analysis of the solids after redissolution in nitric acid showed traces of potassium, boron, calcium and lithium, and large amount of sodium and chloride (Table A. 7 in Supplementary Information). This is attributed to the colloidal nature of $Mg(OH)_2$ which behaves like a sponge entrapping large quantities of species such as sodium and chloride. The colloidal precipitate is also responsible for filtration issues due to coagulation and flocculation phenomena ([10], [11], [43]). The highest weight of solid measured after processing the non-pretreated brine (26.4 g for the non-pretreated brine vs. 21.3 g for the boron-depleted brine) indicates that the presence of boron increases impurities co-precipitation in the solid. Elemental and XRD analyses evidenced that the solid produced from the boron-depleted brine was composed of 73% sodium chloride and 16.4% magnesium hydroxide (Figure 5 (a)). Unfortunately, calcium hydroxide was not identified in the X-Ray diffractograms, which was attributed to the very low initial concentration of calcium within the brine compared to that reported by Nieto et al. [20]. The purity of $Mg(OH)_2$ in the solid was not high enough to envisage magnesium valorization in industry. Therefore, the solid was washed with deionized water at room temperature (22±2 °C) to remove NaCl impurities. Then, the solid was dried and characterized by XRD. Figure 5 (b) shows that the solid is mainly composed of $Mg(OH)_2$ with purity of 71.2% determined by elemental analyses. This indicates that additional work must be done to improve the solid washing or to identify alternative purification strategies.

(a)

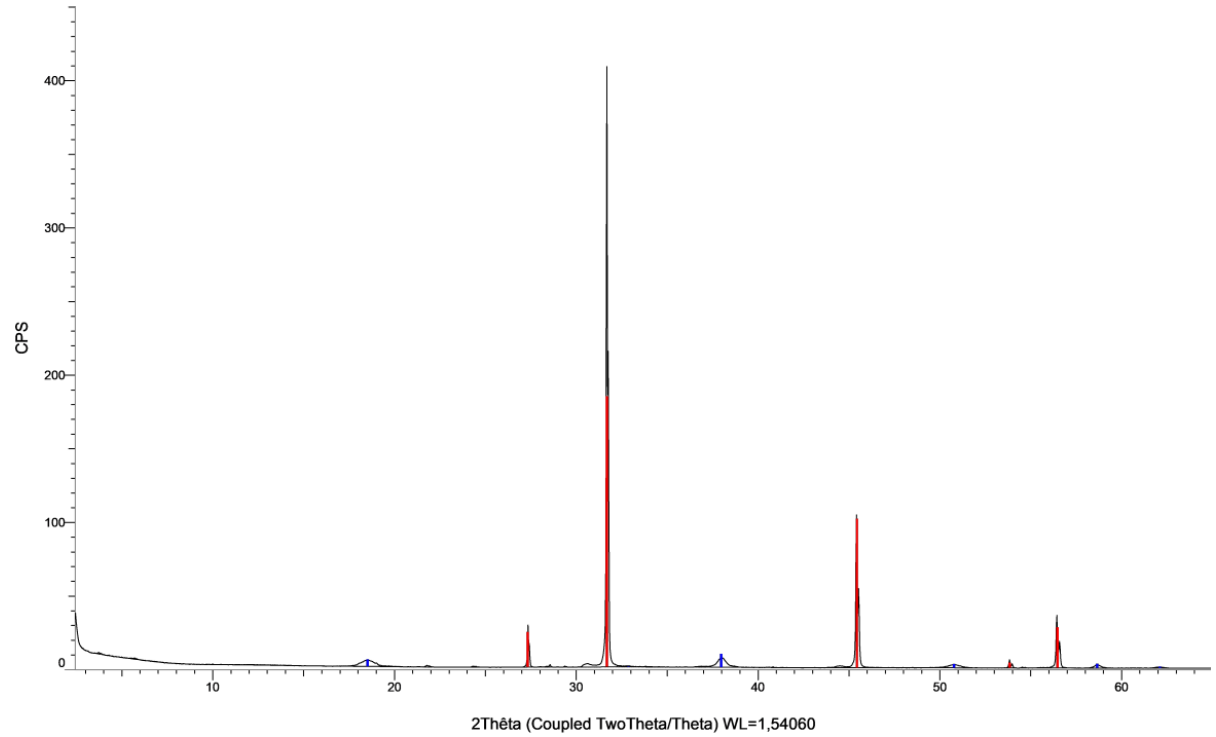

(b)

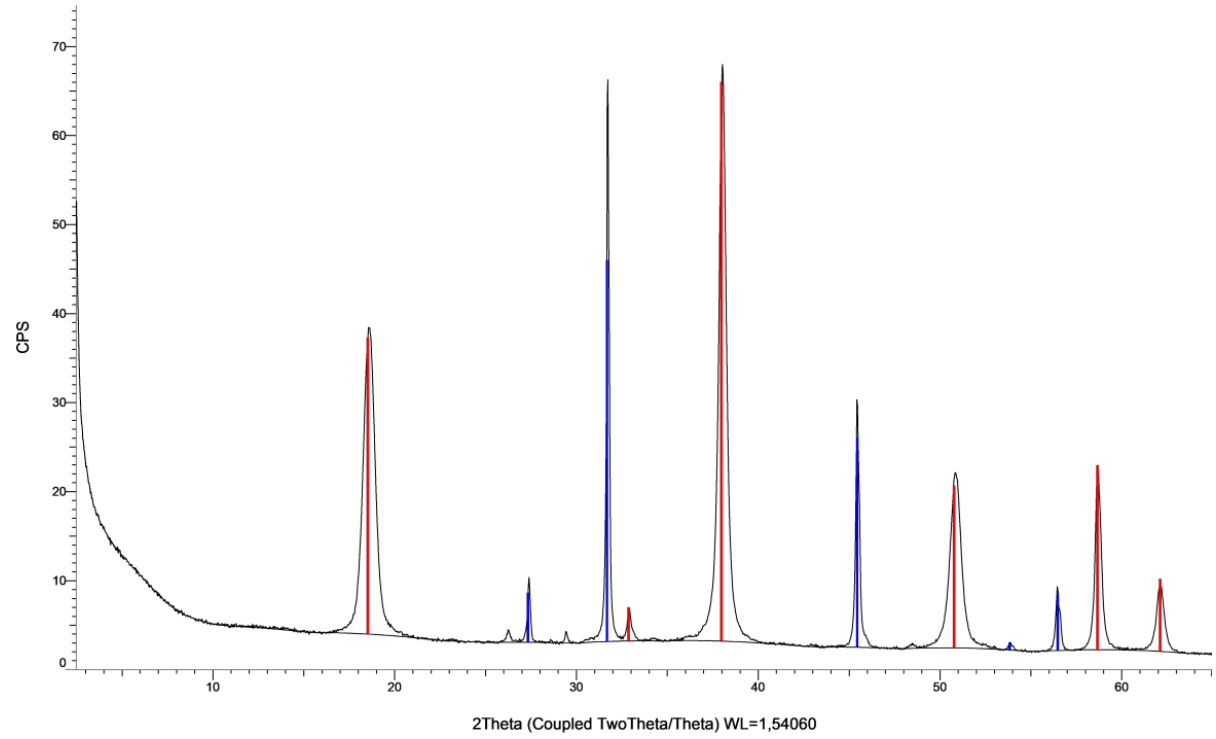

Figure 5: (a) XRD pattern of the solid obtained after magnesium and calcium removal (in black). Reference XRD patterns of NaCl (in red) and $Mg(OH)_2$ (in blue), (b) XRD pattern of the solid obtained after washing (in black). Reference patterns of $Mg(OH)_2$ (in red) and NaCl (in blue).

3.4. Sodium, potassium and lithium separation

In stage II of the electrodialysis (Figure A. 2 in Supporting information), the middle compartment of the cell was fed with only the boron-depleted brine free of magnesium and calcium, *i.e.* the boron-depleted brine leaving stage I (see brines composition before and after stage II in Table 3). Water reduction in the cathodic compartment was responsible for the increase of the catholyte pH and its oxidation in the anodic compartment decreased the anolyte pH, as expected (Equations 6 and 7). Three consecutive electrodialysis experiments were performed until the voltage and the current reached 30 V and ~ 0 A, respectively, (see pH in the three compartments of the electrodialysis cell, voltage, current and concentrations of sodium, potassium and lithium in the middle compartment after each experiment for the boron depleted brine in Table A. 8 in Supplementary Information).

Figure A. 3 in Supplementary Information indicates that sodium, lithium and potassium exist mainly in the brine as Na^+, Li^+ and K^+ at the natural pH of that processed brine (Table 3). During the electrodialysis, these cations and the anions (Cl^- and SO_4^{2-}) migrate from the middle compartment to the cathodic and anodic the compartments, respectively. Therefore, their concentration in the middle compartment is significantly reduced. Figure 6 shows the normalized concentrations (C/C_0) of sodium, lithium and potassium in the brines as a function of the circulated charge per liter of brine. Sodium, lithium and potassium concentrations decrease with the extent of the electrodialysis because Na^+, Li^+ and K^+ cations are transferred from the middle compartment to the cathodic compartment. However, lithium concentration increases at 190,000 C L^{-1} in the brine. This is attributed to the reduction of water volume *via* electroosmosis as previously mentioned.

At the end of the electrodialysis, potassium was removed from the brine while a certain amount of sodium and lithium still remained in the middle compartment (Table 3). Therefore, more energy is needed to remove these residual concentrations.

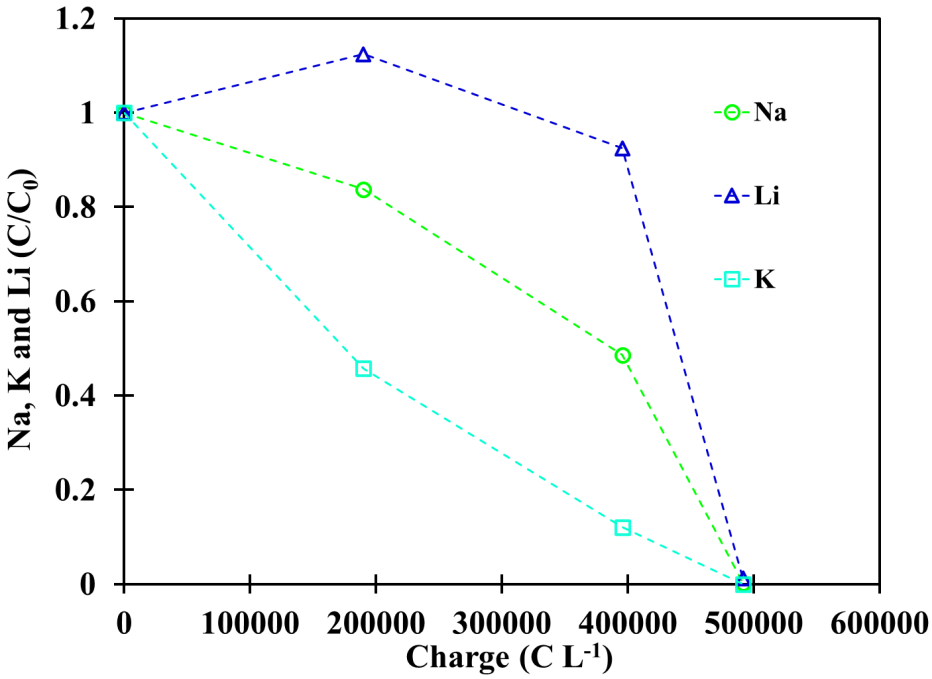

Figure 6: Normalized concentrations of sodium, lithium and potassium in the middle compartment as a function of the circulated charge per liter of brine.

Table 4 shows the separation coefficient between different cations within the brine as a function of the extent of the electrodialysis. F_{Na-K} and F_{Li-K} values are greater than 1. Therefore, K^+ migration through the CEM is more important than Na^+ and Li^+. Additionally, Na^+ transfer through the CEM occurs preferentially compared to Li^+ since F_{Na-Li} values are lower than 1. Hence, it can be inferred that cations migrate from the middle compartment to the cathodic compartment through the CEM following this order: $K^+ > Na^+ > Li^+$. This migration order is supported by hydration free energy of cations which the order is the opposite of that of the separation coefficient : $K^+ < Na^+ < Li^+$ [44]. Similar results were reported by Nieto et al. [14].

Table 4: Separation coefficients of K^+, Na^+ and Li^+ as a function of the circulated charge per liter of brine.

F_{Na-K}	F_{Na-Li}	F_{Li-K}	Charge (C L^{-1})
1.8	0.7	2.5	189,900
4.0	0.5	7.6	395,460
-	0.2	-	491,490

After stage II, the total dissolved solid amounts (TDS) in the brine was 0.7 g L^{-1}. The energy consumption during sodium separation from the boron-depleted brine leaving stage I was 0.53 kWh L^{-1}, which is ten times greater than the energy need for magnesium and calcium removal in stage I. This is attributed to the high concentration of sodium in the brine.

3.5. Sodium carbonate production

After each electrodialysis experiment, CO_2 was bubbled at 2 L min^{-1} for 7 hours in the catholyte containing the transferred K^+, Na^+ and Li^+ cations in order to precipitate sodium as sodium bicarbonate ($NaHCO_3$) or sodium carbonate (Na_2CO_3). Therefore, three precipitation experiments were performed with the catholyte obtained from the non-pretreated brine free of magnesium and calcium. Since the precipitation experiments were the same, only data of the first precipitation experiment with the catholyte obtained from the brine were reported in this work. This catholyte was composed of 58,252 mg L^{-1} sodium, 289 mg L^{-1} lithium, 11,088 mg L^{-1} potassium and 8.5 g L^{-1} carbonate anions (CO_3^{2-}) before CO_2 bubbling. At the beginning of the precipitation experiment, the temperature increased from 25 °C to 43 °C after 30 min of CO_2 bubbling. This energy could be recovered in industrial plants. As the catholyte was alkaline (pH=13.4), CO_2 bubbling was responsible for the decrease of pH in the cathodic compartment (Figure 9). This is explained by the reaction between CO_2 and OH^- to form bicarbonate anions (Equation 20). In the presence of water, CO_2 is also converted into carbonate or hydrogene carbonate (Equations 21 and 22).

$$CO_2 + OH^- \rightleftarrows HCO_3^- \quad (20)$$

$$CO_2 + H_2O \rightleftarrows CO_3^{2-} + 2H^+ \quad (21)$$

$$CO_2 + H_2O \rightleftarrows H_2CO_3 \quad (22)$$

Figure 7 indicates that bicarbonate (HCO_3^-) content is higher at pH=7−9, while carbonate (CO_3^{2-}) is the only species in solution at pH above 11. These bicarbonate and carbonate anions can precipitate K^+, Na^+ and Li^+ cations according to Equations 23−27 [28]. Therefore, CO_2 bubbling should be performed until pH=7−9 in order to precipitate sodium as sodium bicarbonate ($NaHCO_3$) and prevent the precipitation of lithium carbonate and potassium carbonate at pH above 11 since lithium carbonate exhibits the lowest solubility in water (Table A. 6 in Supporting Information).

$$2\,Na^+ + CO_3^{2-} \rightleftarrows Na_2CO_{3(S)} \quad (23)$$

$$Na^+ + HCO_3^- \rightleftarrows NaHCO_{3(S)} \quad (24)$$

$$K^+ + CO_3^{2-} \rightleftarrows K_2CO_{3(S)} \quad (25)$$

$$K^+ + HCO_3^- \rightleftarrows KHCO_{3(S)} \quad (26)$$

$$Li^+ + CO_3^{2-} \rightleftarrows Li_2CO_{3(S)} \quad (27)$$

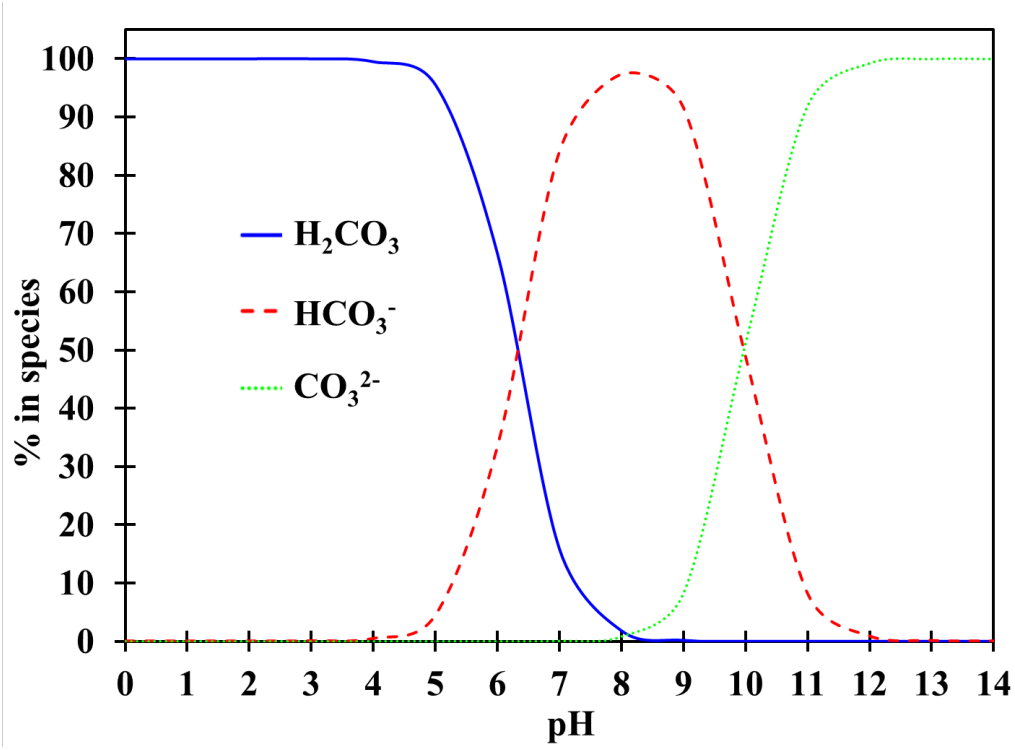

Figure 7: Carbonate speciation in pure water as a function of pH. 0.1 mol L^{-1} carbonate was used for speciation calculations.

Figure 9 evidences that bicarbonate and sodium bicarbonate are the only carbonate species in the catholyte at pH=7.7. Lithium carbonate, sodium carbonate, potassium carbonate and potassium bicarbonate species are not reported in Figure 9 because of the lack of their thermodynamic data in the database Minteq.V4 [29]. Nevertheless, these speciation diagrams provides consistent experimental condition to selectively precipitate sodium. Therefore, CO_2 was bubbled until the pH of the catholyte reached 7.7 (Figure 8). As shown in Figure 8, sodium concentration decreases slightly until pH=9.8 and exhibits sharp decrease at pH=9.8−7.7. The difference of behavior regarding sodium precipitation as a function of pH is attributed to carbonate anions speciation. Indeed, the increase in carbonate concentration from 8.5 g L^{-1} to 69.5 g L^{-1} during the CO_2 bubbling is responsible for huge amount of bicarbonate production (see Figure 8 for the increase in carbonate concentration and Figure 9 for the increase in the concentration of bicarbonate). Hence, the produced bicarbonate anions precipitate significantly sodium as sodium bicarbonate at pH=9.8−7.7 (Figure 8). Lithium and potassium concentrations in the catholyte decreased at pH=13.4−9.8 during CO_2 bubbling. Conversely, their concentrations increase at pH below 9.8 (Figure 8). This can be explained by the formation of lithium carbonate, potassium carbonate and potassium bicarbonate species which can precipitate when their solubilities are reached in some pH regions (see the solubility of these salts at 25 °C in Table A. 6 in Supporting information).

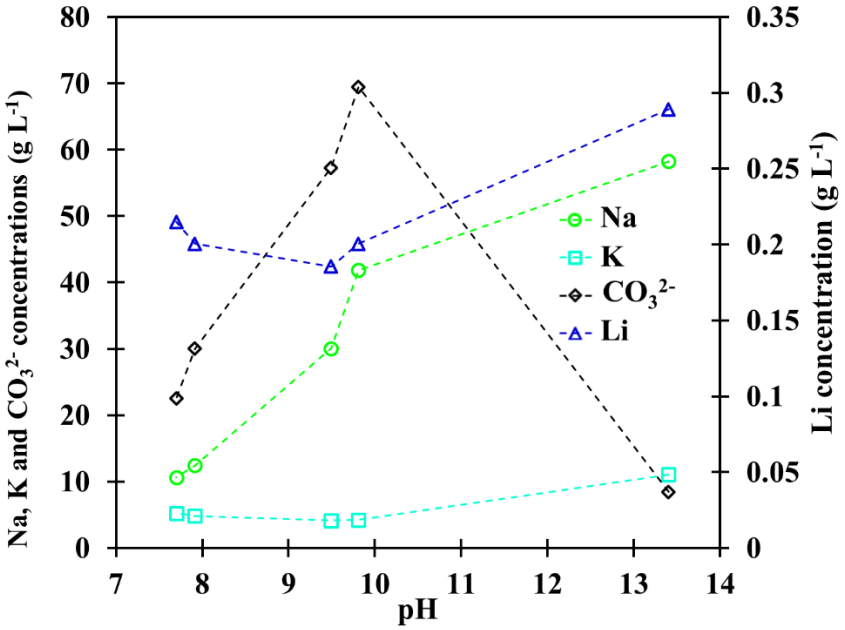

Figure 8: Experimental sodium, lithium, potassium and carbonate anions (CO_3^{2-}) concentrations in the catholyte during CO_2 bubbling as a function of pH (read pH evolution during CO_2 bubbling from right to left)

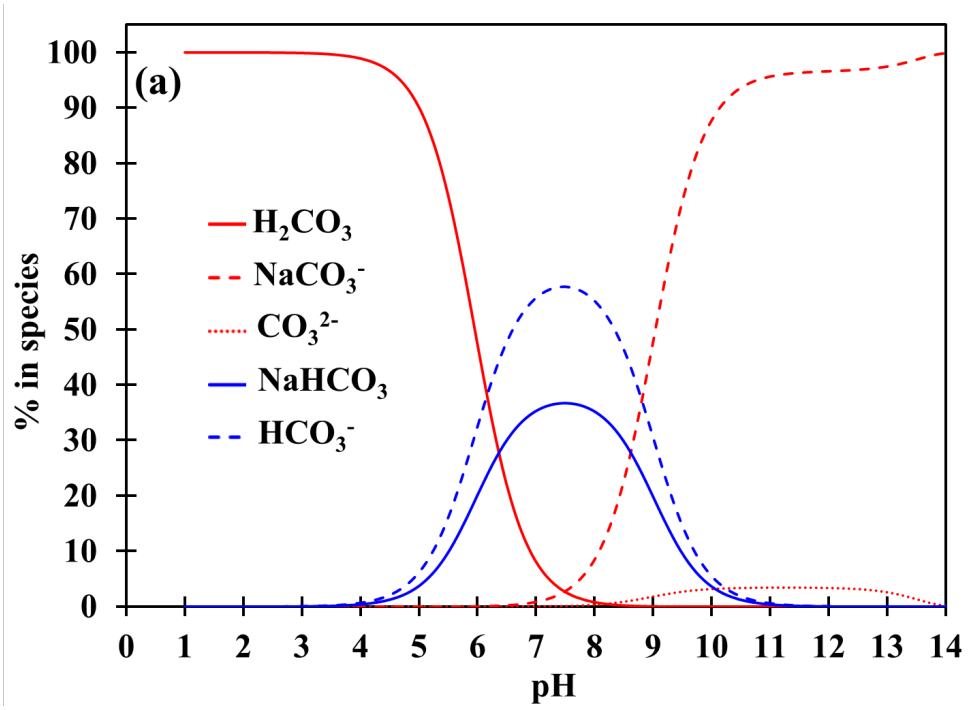

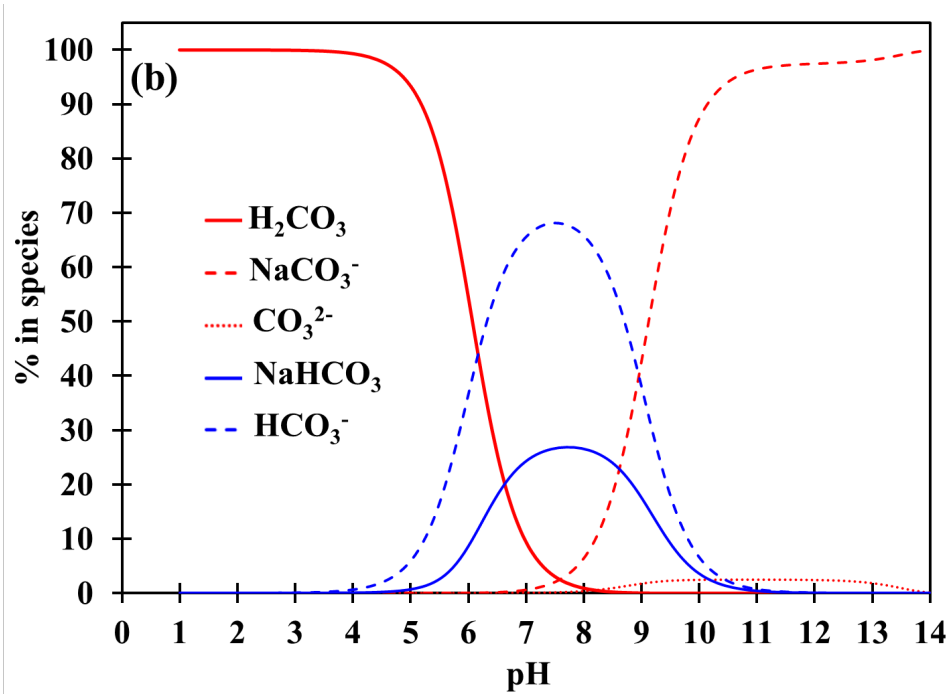

Figure 9: Carbonate speciation as a function of pH (a) before CO_2 bubbling (carbonate concentration= 8.5 g L^{-1}) and (b) at the maximum concentration of carbonate (69.5 g L^{-1}) obtained during CO_2 bubbling.

After the three precipitation experiments for the catholyte obtained from the boron-depleted brine free of magnesium and calcium, the solids were recovered by filtration under vacuum and heated at 110 °C for 24 hours to convert $NaHCO_3$ into Na_2CO_3 [45]. This convertion of $NaHCO_3$ into Na_2CO_3 can be an opportunity of CO_2 recycling in the process (Equation 28).

$$NaHCO_{3(s)} \rightarrow Na_2CO_{3(s)} + CO_{2(g)} + H_2O_{(g)} \quad (28)$$

Afterwards, 82.7 g of solid were harvested. Elemental analyses showed that the solid was composed of 41.2% sodium (Na_2CO_3 purity=95%), 0.4% potassium and 0.1% lithium. Therefore, the solid was washed with deionized water at 0 °C to minimize redissolution of Na_2CO_3 and remove the impurities. The washed solid was dried as previously. XRD analysis showed that the solid was only composed of Na_2CO_3 (Figure 10). The purity of Na_2CO_3 (99.99%) was confirmed by elemental analyses.

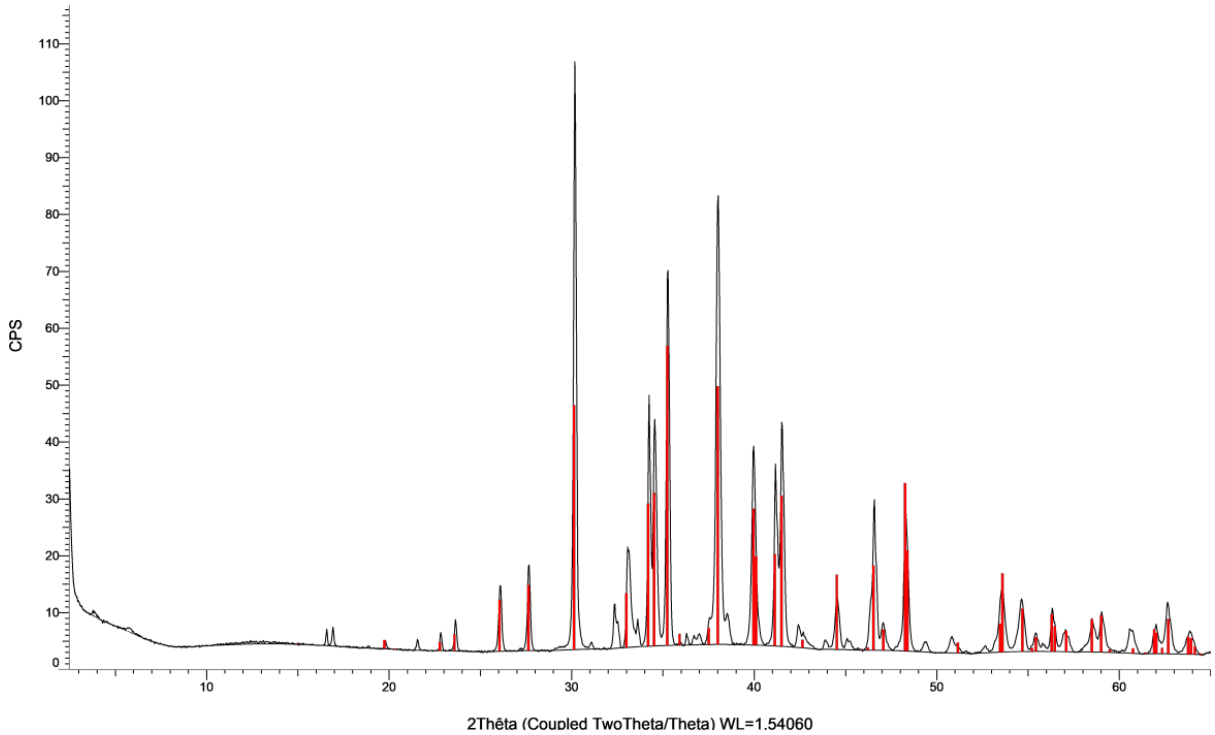

Figure 10: XRD pattern of the solid after washing (in black). Reference XRD patterns of sodium carbonate in red. The solid was obtained by precipitation of the catholyte in stage II.

3.6. Lithium separation

Lithium extraction from the catholyte obtained after sodium precipitation in stage II was performed by implementing stage III of the electrodialysis process. The solution contained 986 mg L^{-1} lithium, 8,332 mg L^{-1} potassium and 27,602 mg L^{-1} sodium and fed the middle compartment of the electro-membrane cell (Figure A. 2 (c) in Supporting Information). The cathodic and the anodic compartment were fed by 0.1 mol L^{-1} Li_2CO_3 and 0.5 mol L^{-1} Na_2CO_3, respectively. The experiment was performed at 150 A m^{-2} for 11 hours. Table 5 reports the evolution of pH in the three compartments of the electro-membrane cell, voltage, current and, concentrations of lithium, sodium and potassium in the middle compartment as a function of the electrodialysis extent. During the experiment, the pH in the cathodic compartment increases due to water reduction (Equation 7) and the pH in the anodic compartment decreases because of water oxidation (Equation 6). At the end of the electrodialysis process, sodium, lithium and potassium were transferred from the middle compartment to the cathodic compartment (Table 5). The separation coefficients of the cations were similar to those in stage II and cations migrate through the CEM as follows: $K^+ > Na^+ > Li^+$. The higher concentrations in sodium and potassium, and the more preferential migration of sodium and potassium than lithium is a disadvantage for efficient lithium recovery. Torres et al. reported that low ratio [Na]/[Li] improves the lithium recovery by electrodialysis [46].

Table 5: Evolution of pH in the three compartments of stage III, voltage, current and, concentrations of lithium, sodium and potassium in the middle compartment as a function of the electrodialysis extent.

Time (min)	Charge (C L^{-1})	pH middle	pH of anolyte	pH of catholyte	Na^+ Middle compartment (mg L^{-1})	Li^+ Middle compartment (mg L^{1})	K^+ Middle compartment (mg L^{-1})	Current (A)	Voltage (V)
0	0	8.4	11.1	10.1	27,602	986	8,332	0.75	4.4
249	56,025	8.9	10.2	12.9	20,614	838	3,420	0.75	4.4
434	97,650	9.4	10.0	12.9	10,287.5	605	627.5	0.75	4.7
691	155,475	10.5	9.9	13.0	**0**	**0**	**0**	0	30

3.7. Lithium carbonate production

Sodium, lithium and potassium concentrations in the catholyte at the end of stage III (25,375 mg L^{-1} sodium, 870 mg L^{-1} lithium and 3,589 mg L^{-1} potassium) were lower than those in the middle compartment before the experiment (Table 5). This is attributed to the increase in the volume of the catholyte due to electroosmosis as previously discussed. CO_2 was bubbled in the catholyte at 2.5 L min^{-1} and 25 °C for 1h30 until the pH reached 10 so that carbonate concentration was high enough to precipitate lithium as lithium carbonate (Figure 7). No precipitation was observed because lithium concentration (870 mg L^{-1}) was much lower than 2.4 g L^{-1} (solubility of lithium carbonate at 25 °C=13 g L^{-1} which is equivalent to 2.4 g L^{-1} lithium). Therefore, lithium concentration must be increased beyond 2.4 g L^{-1}. The catholyte was evaporated at 90 °C under stirring until the volume was reduced by four. Table 6 gathers the concentrations of lithium, potassium and sodium during the evaporation step. At the end of the evaporation, lithium, potassium and sodium concentrations should be 3,424 mg L^{-1}, 13,120 mg L^{-1}, and 114,016 mg L^{-1}, respectively. However, Table 6 indicates that sodium and lithium concentrations significantly were much lower. Indeed, during evaporation lithium carbonate and sodium carbonate crystallized since Li_2CO_3 and Na_2CO_3 solubilities at 90 °C reaches 8.1 g L^{-1} and 447 g L^{-1}, respectively, which are equivalent to 1.5 g L^{-1} lithium and 192.3 g L^{-1} sodium ([28], [47]). The crystals were recovered by filtration and the solid was dried at 100 °C for 24 hours. XRD analysis of the solid showed the presence of Li_2CO_3 and Na_2CO_3 (Figure 11 (a)). The purity of the lithium carbonate reached 65%, which is too low for battery applications since lithium carbonate battery-grade ranges between 99.5% and 99.95% [9].

The crystallized solid was washed with deionized water at 90 °C to minimize the redissolution of Li_2CO_3 and remove Na_2CO_3 impurities. The washed solid was dried as previously described. Figure 11 (b) evidences that there is no significant difference between the diffractograms of the washed solid and lithium carbonate. Elemental analyses of the solid indicated that lithium carbonate purity was 99.9%.

Table 6: Composition of catholyte (1) before evaporation, (2) when the volume of catholyte was reduced by 2 during evaporation and (3) when the volume of the catholyte was reduced by 4 during evaporation.

	Concentration of cation (mg L^{-1})		
Catholyte	K^+	Li^+	Na^+
(1)	3,280	856	28,505
(2)	6,194	1,533	53,013
(3)	12,946	1,866	103,398

(a)

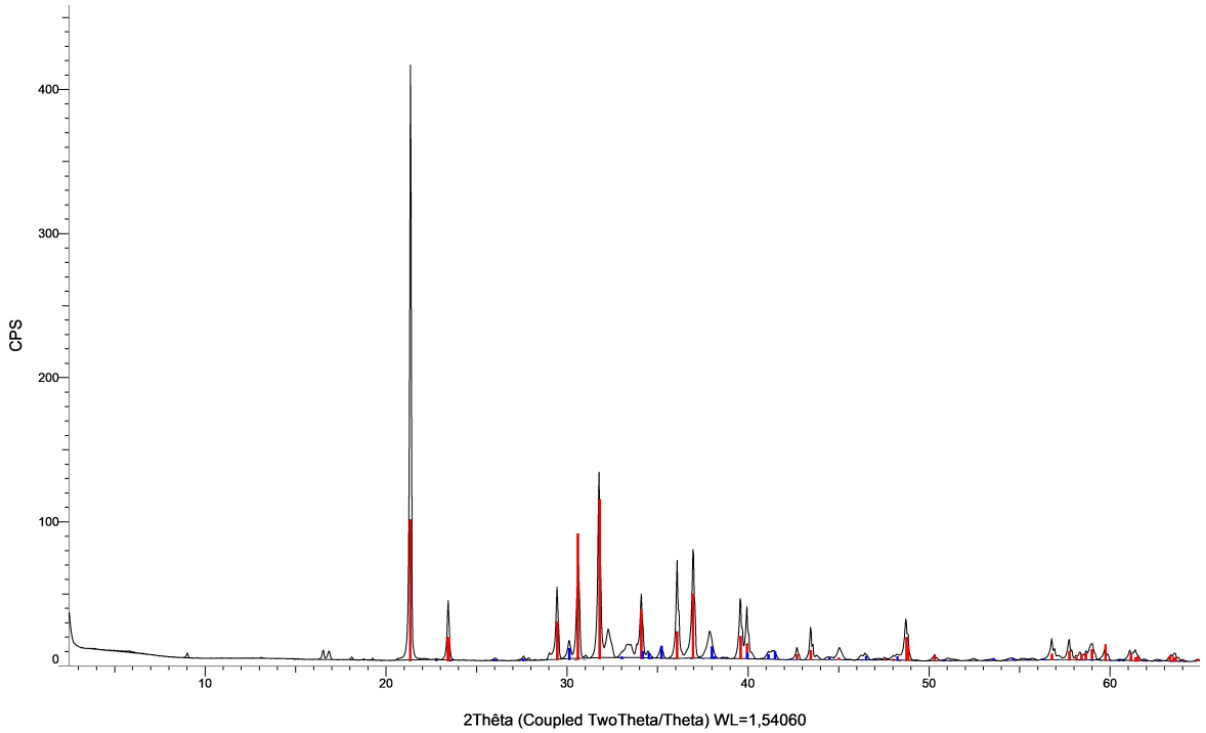

(b)

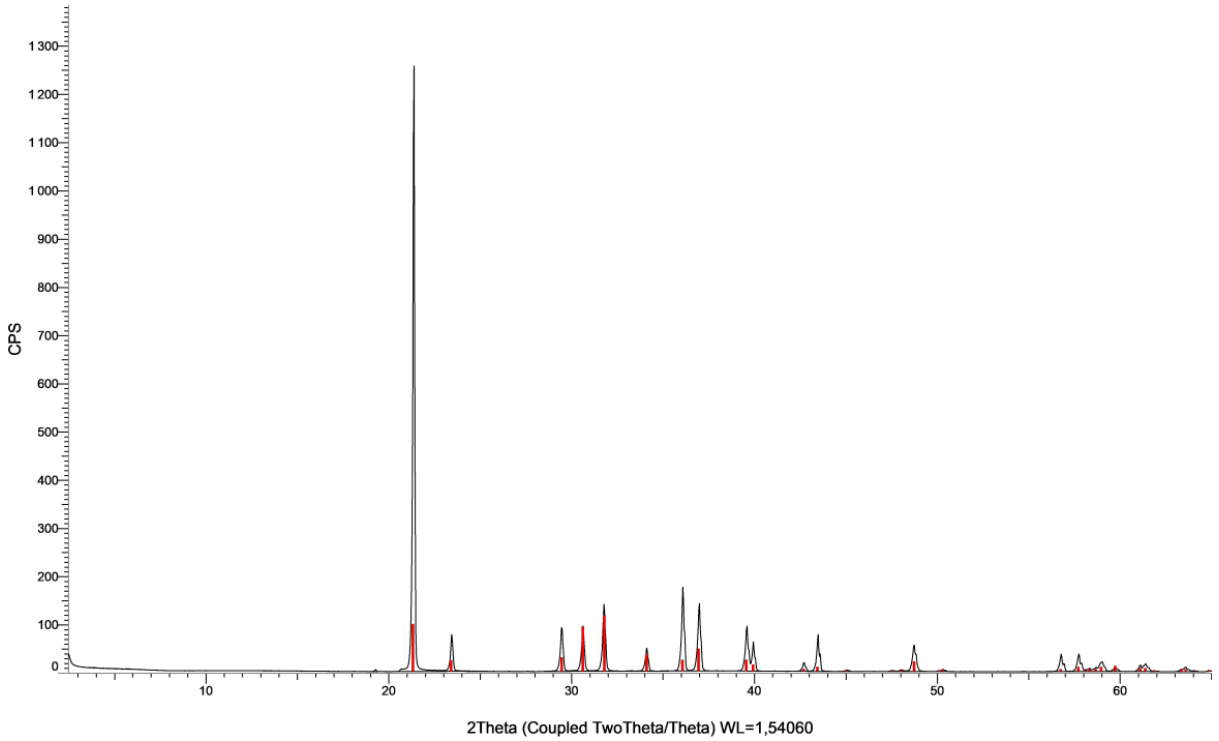

Figure 11 : (a) XRD pattern of the crystallized solid from the catholyte of stage III (in black), and reference XRD patterns of lithium carbonate (in red) and sodium carbonate (in blue), (b) XRD pattern of the washed solid (in black) and reference XRD patterns of lithium carbonate (in red). The solid was obtained by crystallization of the catholyte in stage III

4. Conclusion

Direct lithium extraction technologies are becoming a reference for sustainable lithium production from brines. Among these technologies, electrodialysis is a relevant technique that could be implemented to extracting lithium efficiently and selectively. However, the numerous lithium-rich brines components make lithium extraction by electrodialysis very challenging. Indeed, boron, sodium, potassium, magnesium and calcium should be removed before lithium processing. Despite the combination of electrodialysis and precipitation operations addressed in our previous research [21], boron contributed to increase the impurities in the co-valorized salts. Therefore, this paper carried out boron extraction from native brine by 2 mol L^{-1} 2-butyloctan-1-ol diluted in kerosene before performing the electrodialysis process allowing to investigate the influence of boron extraction on the performance of the whole process.

High extraction efficiency of boron (90%) was reached by performing 8 batch extractions with l L of brine and 4 L of the extraction solvent at the initial pH of the brine (pH=7.5) and 25 °C. Boron was then stripped by 0.1 mol L^{-1} sodium hydroxide in order to selectively produce borax ($Na_2B_4O_7•2H_2O$, purity=99%). Thereafter, the non-pretreated brine and the boron-depleted brine were processed by electrodialysis. This study showed that boron extraction before the electrodialysis experiments contribute to:

- Decrease the impurities in stage I by 18% allowing to reduce the amount of water needed to wash $Mg(OH)_2$ obtained from the boron-depleted brine.
- Reduce the energy consumption in stage I by 17%. This was explained by the formation of neutral species of boron-magnesium and boron-calcium that keep magnesium and calcium in solution and then, increase the energy consumption required to remove magnesium and calcium.

Figure 12 depicts the flowsheet gathering solvent extraction of boron, magnesium and sodium separation and battery-grade lithium carbonate production. The by-products are borax, magnesium hydroxide and sodium carbonate. By combining solvent extraction with the electrodialysis operation, magnesium hydroxide (purity=71.2%), sodium carbonate (purity=99.99%) and lithium carbonate (purity=99.9%) were obtained in stages I, II and III of the electrodialysis process. After stage II, the TDS was decreased by 99.8% since the TDS in the native brine was initially 304.5 g L^{-1} and it reached 0.7 g L^{-1} at the end of stage II. Then, the produced low salinity water can be employed for solids washing and the electrodialysis operations. It can also be envisaged to employ the low salinity water in agriculture.

This research highlights the critical importance of boron extraction for efficient lithium carbonate production by electrodialysis because boron removal contributes to reducing the operating cost *via* significant decrease of the impurities in the produced salts and the energy consumption by 17%. This work also addresses the intricate physicochemistry of magnesium, calcium, sodium and lithium speciation in alkaline solutions or carbonate-rich solutions. Unlike the conventional lithium extraction processes, this work points out the relevance of the co-valorization of boron, magnesium and sodium in lithium plants, which reduces the waste production in this industry.

The large amount of sodium in the brines entails huge energy consumption to remove sodium increasing the operating costs. However, the co-produced sodium carbonate may make this process economically beneficial. The high content of sodium in brine is also responsible for the reduction of the efficiency of lithium extraction in stage III since sodium migrates more preferentially than lithium. Therefore, more selective membranes towards lithium should be developed and employed to avoid this issue and reduce the impurity in the produced lithium carbonate. Counter-current washing could be an alternative to enhance the purity of $Mg(OH)_2$ obtained in stage I. Higher concentration of lithium in the cathodic compartment of stage III should allow to precipitating lithium carbonate solely by CO_2 bubbling instead of evaporation. This could be achieved by increasing the ratio between the volume of aqueous phase employed in the middle compartment and the catholyte.

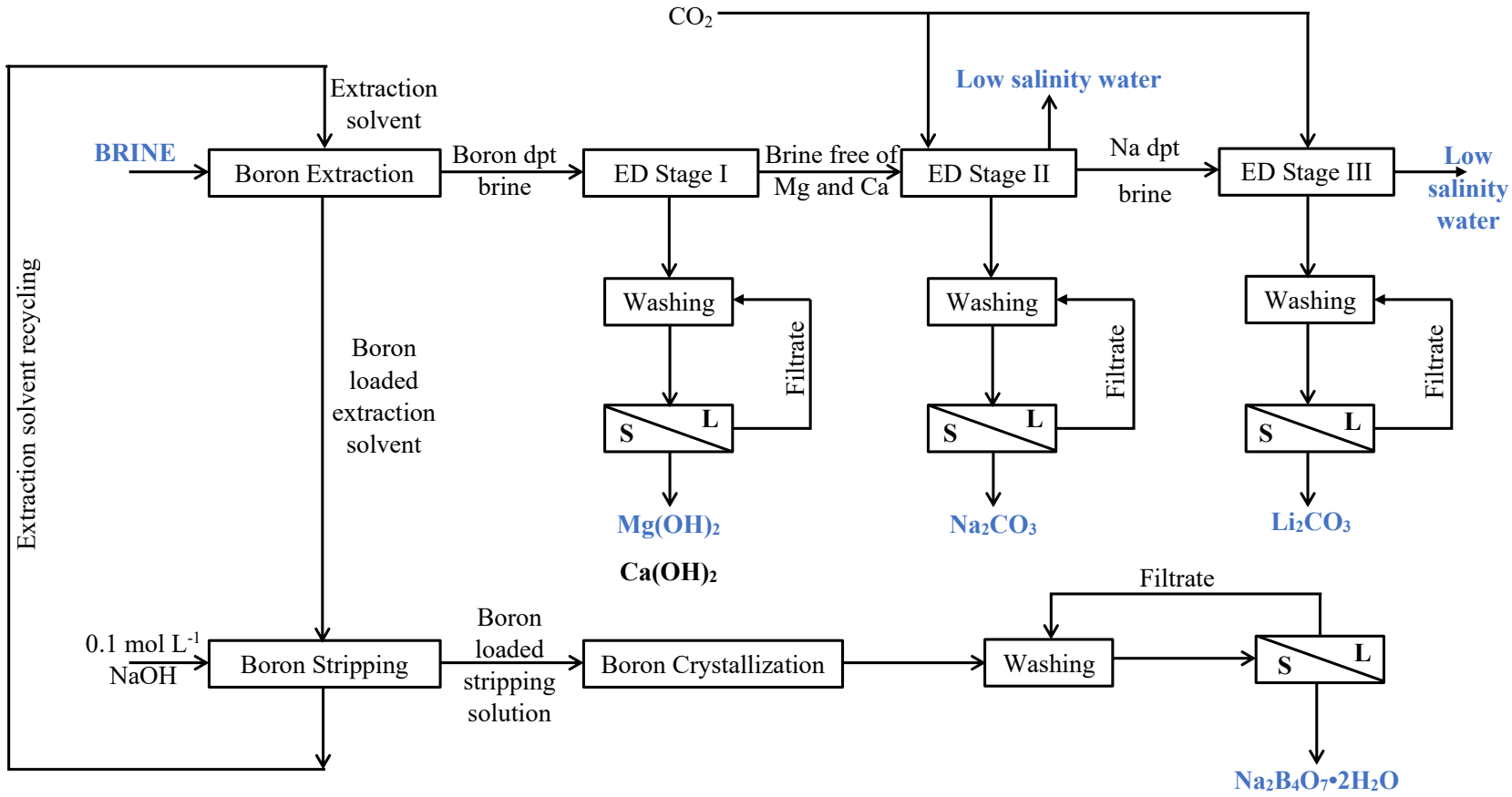

Figure 12: Flowsheet of the overall process for borax, magnesium hydroxide, sodium carbonate and battery-grade lithium carbonate production from the native brine (dpt denotes depleted.)

References

[1] USGS, “Mineral commodity summaries 2024,” 2024. doi: 10.3133/mcs2024.

[2] P. W. Gruber, P. A. Medina, G. A. Keoleian, S. E. Kesler, M. P. Everson, and T. J. Wallington, “Global Lithium Availability,” *Journal of Industrial Ecology*, vol. 15, no. 5, pp. 760–775, 2011, doi: 10.1111/j.1530-9290.2011.00359.x.

[3] B. Swain, “Recovery and recycling of lithium: A review,” *Separation and Purification Technology*, vol. 172, pp. 388–403, Jan. 2017, doi: 10.1016/j.seppur.2016.08.031.

[4] V. Flexer, C. F. Baspineiro, and C. I. Galli, “Lithium recovery from brines: A vital raw material for green energies with a potential environmental impact in its mining and processing,” *Science of The Total Environment*, vol. 639, pp. 1188–1204, Oct. 2018, doi: 10.1016/j.scitotenv.2018.05.223.

[5] F. Meng, J. McNeice, S. S. Zadeh, and A. Ghahreman, “Review of Lithium Production and Recovery from Minerals, Brines, and Lithium-Ion Batteries,” *Mineral Processing and Extractive Metallurgy Review*, vol. 42, no. 2, pp. 123–141, Feb. 2021, doi: 10.1080/08827508.2019.1668387.

[6] A. Chagnes, *Lithium Process Chemistry : Resources, Extraction, Batteries, and Recycling*. Elsevier Science, 2015. Accessed: Jan. 25, 2022. [Online]. Available: http://univ.scholarvox.com.bases-doc.univ-lorraine.fr/catalog/book/docid/88829473

[7] P. K. Choubey, M. Kim, R. R. Srivastava, J. Lee, and J.-Y. Lee, “Advance review on the exploitation of the prominent energy-storage element: Lithium. Part I: From mineral and brine resources,” *Minerals Engineering*, vol. 89, pp. 119–137, Apr. 2016, doi: 10.1016/j.mineng.2016.01.010.

[8] M. L. Vera, W. R. Torres, C. I. Galli, A. Chagnes, and V. Flexer, “Environmental impact of direct lithium extraction from brines,” *Nat Rev Earth Environ*, vol. 4, no. 3, Art. no. 3, Mar. 2023, doi: 10.1038/s43017-022-00387-5.

[9] O. Murphy and M. N. Haji, “A review of technologies for direct lithium extraction from low Li+ concentration aqueous solutions,” *Front. Chem. Eng.*, vol. 4, Nov. 2022, doi: 10.3389/fceng.2022.1008680.

[10] L. Semerjian and G. M. Ayoub, “High-pH–magnesium coagulation–flocculation in wastewater treatment,” *Advances in Environmental Research*, vol. 7, no. 2, pp. 389–403, Jan. 2003, doi: 10.1016/S1093-0191(02)00009-6.

[11] Q. Yuan, Z. Lu, P. Zhang, X. Luo, X. Ren, and T. D. Golden, “Study of the synthesis and crystallization kinetics of magnesium hydroxide,” *Materials Chemistry and Physics*, vol. 162, pp. 734–742, Jul. 2015, doi: 10.1016/j.matchemphys.2015.06.048.

[12] J. A. Stewart, “Potassium Sources, Use, and Potential,” in *Potassium in Agriculture*, John Wiley & Sons, Ltd, 1985, pp. 83–98. doi: 10.2134/1985.potassium.c5.

[13] M. Xue *et al.*, “Flame retardant effect of lignin/carbon nanohorns/potassium carbonate composite flame retardant on fir pretreated under different methods,” *Thermochimica Acta*, vol. 731, p. 179641, Jan. 2024, doi: 10.1016/j.tca.2023.179641.

[14] C. H. Díaz Nieto, K. Rabaey, and V. Flexer, “Membrane electrolysis for the removal of Na+ from brines for the subsequent recovery of lithium salts,” *Separation and Purification Technology*, vol. 252, p. 117410, Dec. 2020, doi: 10.1016/j.seppur.2020.117410.

[15] F. de Mestral and R. A. L. Drew, “Calcium phosphate glasses and glass-ceramics for medical applications,” *Journal of the European Ceramic Society*, vol. 5, no. 1, pp. 47–53, Jan. 1989, doi: 10.1016/0955-2219(89)90008-3.

[16] T. Turkbay, J. Bongono, T. Alix, B. Laratte, and B. Elevli, “Prior knowledge of the data on the production capacity of boron facilities in Turkey,” *Cleaner Engineering and Technology*, vol. 10, p. 100539, Oct. 2022, doi: 10.1016/j.clet.2022.100539.

[17] J. Farahbakhsh *et al.*, “Direct lithium extraction: A new paradigm for lithium production and resource utilization,” *Desalination*, vol. 575, p. 117249, Apr. 2024, doi: 10.1016/j.desal.2023.117249.

[18] A. Khalil, S. Mohammed, R. Hashaikeh, and N. Hilal, “Lithium recovery from brine: Recent developments and challenges,” *Desalination*, vol. 528, p. 115611, Apr. 2022, doi: 10.1016/j.desal.2022.115611.

[19] S. Gmar and A. Chagnes, “Recent advances on electrodialysis for the recovery of lithium from primary and secondary resources,” *Hydrometallurgy*, vol. 189, p. 105124, Nov. 2019, doi: 10.1016/j.hydromet.2019.105124.

[20] C. H. Díaz Nieto, N. A. Palacios, K. Verbeeck, A. Prévoteau, K. Rabaey, and V. Flexer, “Membrane electrolysis for the removal of Mg2+ and Ca2+ from lithium rich brines,” *Water Research*, vol. 154, pp. 117–124, May 2019, doi: 10.1016/j.watres.2019.01.050.

[21] W. R. Torres, C. H. Díaz Nieto, A. Prévoteau, K. Rabaey, and V. Flexer, “Lithium carbonate recovery from brines using membrane electrolysis,” *Journal of Membrane Science*, vol. 615, p. 118416, Dec. 2020, doi: 10.1016/j.memsci.2020.118416.

[22] C. H. Díaz Nieto, J. A. Kortsarz, M. L. Vera, and V. Flexer, “Effect of temperature, current density and mass transport during the electrolytic removal of magnesium ions from lithium rich brines,” *Desalination*, vol. 529, p. 115652, May 2022, doi: 10.1016/j.desal.2022.115652.

[23] P. M. Brown and S. J. Beckerman, “Production of lithium metal grade lithium chloride from lithium-containing brine,” US4980136A, Dec. 25, 1990 Accessed: Jan. 26, 2022. [Online]. Available: https://patents.google.com/patent/US4980136/en?oq=PRODUCTION+OF+LITHIUM+METAL+GRADE+LITHIUM+CHLORIDE+FROM+LITHIUM+CONTAINING+BRINE

[24] D. E. Garrett, “Part 1 - Lithium,” in *Handbook of Lithium and Natural Calcium Chloride*, D. E. Garrett, Ed., Oxford: Academic Press, 2004, pp. 1–235. doi: 10.1016/B978-012276152-2/50037-2.

[25] A. F. Kiemde, J. Marin, V. Flexer, and A. Chagnes, “Liquid–liquid extraction of boron from continental brines by 2-butyl-1-octanol diluted in kerosene,” *RSC Adv.*, vol. 14, no. 4, pp. 2170–2181, Jan. 2024, doi: 10.1039/D3RA08045E.

[26] S. Maes, W.-Q. Zhuang, K. Rabaey, L. Alvarez-Cohen, and T. Hennebel, “Concomitant Leaching and Electrochemical Extraction of Rare Earth Elements from Monazite,” *Environ. Sci. Technol.*, vol. 51, no. 3, pp. 1654–1661, Feb. 2017, doi: 10.1021/acs.est.6b03675.

[27] J. Desloover, A. Abate Woldeyohannis, W. Verstraete, N. Boon, and K. Rabaey, “Electrochemical Resource Recovery from Digestate to Prevent Ammonia Toxicity during Anaerobic Digestion,” *Environ. Sci. Technol.*, vol. 46, no. 21, pp. 12209–12216, Nov. 2012, doi: 10.1021/es3028154.

[28] D. W. H. Rankin, "CRC handbook of chemistry and physics, 89th edition, edited by David R. Lide," *Crystallography Reviews*, vol. 15, no. 3, pp. 223–224, Jul. 2009, doi: 10.1080/08893110902764125.

[29] D. L. Parkhurst and C. A. J. Appelo, "Description of input and examples for PHREEQC version 3: a computer program for speciation, batch-reaction, one-dimensional transport, and inverse geochemical calculations," U.S. Geological Survey, Reston, VA, USGS Numbered Series 6-A43, 2013. doi: 10.3133/tm6A43.

[30] C. Shuguang, L. Jun, and L. Bing, "Thermochemistry of teepleite," *Thermochimica Acta*, vol. 376, no. 2, pp. 169–174, Sep. 2001, doi: 10.1016/S0040-6031(01)00562-7.

[31] A. G. Kasikov and A. M. Petrova, "Extraction of sulfuric and hydrochloric acids with macromolecular aliphatic alcohols of varied structure," *Russ J Appl Chem*, vol. 81, no. 12, pp. 2079–2083, Dec. 2008, doi: 10.1134/S1070427208120069.

[32] W. C. Blasdale and C. M. Slansky, "The Solubility Curves of Boric Acid and the Borates of Sodium," *J. Am. Chem. Soc.*, vol. 61, no. 4, pp. 917–920, Apr. 1939, doi: 10.1021/ja01873a043.

[33] "Borax Decahydrate | Multifunctional boric oxide source | U.S. Borax." Accessed: May 27, 2024. [Online]. Available: https://www.borax.com/products/borax-decahydrate

[34] "ICSC 0567 - TETRABORATE DE SODIUM, DECAHYDRATE." Accessed: May 27, 2024. [Online]. Available: https://chemicalsafety.ilo.org/dyn/icsc/showcard.display?p_lang=fr&p_card_id=0567

[35] E. J. Reardon, "Dissociation constants for alkali earth and sodium borate ion pairs from 10 to 50°C," *Chemical Geology*, vol. 18, no. 4, pp. 309–325, Dec. 1976, doi: 10.1016/0009-2541(76)90013-9.

[36] K. Sasaki, K. Toshiyuki, K. Ideta, J. Miyawaki, and T. Hirajima, "Interfacial effects of MgO in hydroxylated calcined dolomite on the co-precipitation of borates with hydroxyapatite," *Colloids and Surfaces A: Physicochemical and Engineering Aspects*, vol. 504, pp. 1–10, Sep. 2016, doi: 10.1016/j.colsurfa.2016.05.044.

[37] Y. Xiong, L. Kirkes, and T. Westfall, "Experimental Determination of Solubilities of Brucite [Mg(OH)2(cr)] in Na2SO4 Solutions with Borate to High Ionic Strengths: Interactions of MgB(OH)4+with Na2SO4," *J Solution Chem*, vol. 47, no. 4, pp. 595–610, Apr. 2018, doi: 10.1007/s10953-018-0742-z.

[38] M. Iwata, T. Tanaka, and M. S. Jami, "Application of Electroosmosis for Sludge Dewatering—A Review," *Drying Technology*, vol. 31, no. 2, pp. 170–184, Jan. 2013, doi: 10.1080/07373937.2012.691592.

[39] D. Wiley and G. F. Weihs, "Electro-osmosis, Overview of," in *Encyclopedia of Membranes*, E. Drioli and L. Giorno, Eds., Berlin, Heidelberg: Springer, 2016, pp. 1–3. doi: 10.1007/978-3-642-40872-4_2079-2.

[40] V. I. Zabolotskii, K. V. Protasov, and M. V. Sharafan, "Sodium chloride concentration by electrodialysis with hybrid organic-inorganic ion-exchange membranes: An investigation of the process," *Russ J Electrochem*, vol. 46, no. 9, pp. 979–986, Sep. 2010, doi: 10.1134/S1023193510090028.

[41] N. Lakshminarayanaiah, "Electroosmosis in Ion-Exchange Membranes," *J. Electrochem. Soc.*, vol. 116, no. 3, p. 338, Mar. 1969, doi: 10.1149/1.2411842.

[42] A. H. Galama, M. Saakes, H. Bruning, H. H. M. Rijnaarts, and J. W. Post, “Seawater predesalination with electrodialysis,” *Desalination*, vol. 342, pp. 61–69, Jun. 2014, doi: 10.1016/j.desal.2013.07.012.

[43] X. Huang *et al.*, “Removal of petroleum sulfonate from aqueous solutions using freshly generated magnesium hydroxide,” *Journal of Hazardous Materials*, vol. 219–220, pp. 82–88, Jun. 2012, doi: 10.1016/j.jhazmat.2012.03.059.

[44] B. Tansel, “Significance of thermodynamic and physical characteristics on permeation of ions during membrane separation: Hydrated radius, hydration free energy and viscous effects,” *Separation and Purification Technology*, vol. 86, pp. 119–126, Feb. 2012, doi: 10.1016/j.seppur.2011.10.033.

[45] M. Mahmoudkhani and D. W. Keith, “Low-energy sodium hydroxide recovery for CO2 capture from atmospheric air—Thermodynamic analysis,” *International Journal of Greenhouse Gas Control*, vol. 3, no. 4, pp. 376–384, Jul. 2009, doi: 10.1016/j.ijggc.2009.02.003.

[46] W. R. Torres, N. C. Zeballos, and V. Flexer, “Effect of [Na+]/[Li+] concentration ratios in brines on lithium carbonate production through membrane electrolysis,” *Faraday Discuss.*, vol. 247, no. 0, pp. 101–124, Oct. 2023, doi: 10.1039/D3FD00051F.

[47] W. Cheng, Z. Li, and F. Cheng, “Solubility of Li2CO3 in Na–K–Li–Cl brines from 20 to 90°C,” *The Journal of Chemical Thermodynamics*, vol. 67, pp. 74–82, Dec. 2013, doi: 10.1016/j.jct.2013.07.024.

SUPPORTING INFORMATION

Direct lithium extraction from natural brines with co-valorization of boron, magnesium and sodium by combining solvent extraction and electrodialysis operations

Abdoul Fattah Kiemde[a], Cesar H. Díaz Nieto[b], Jérôme Marin[a], Victoria Flexer[b]*, Alexandre Chagnes[a]*

[a] *Université de Lorraine, CNRS, GeoRessources, F- 54000 Nancy, France.*

[b] *CIDMEJu, CONICET - Universidad Nacional de Jujuy, Jujuy, Argentina.*

(a) **(b)** **(c)**

Figure A. 1: Setup of solvent extraction experiments (a) before boron extraction, (b) during boron extraction and (c) during boron stripping.

Table A. 1: Concentration of boron as a function of time in the brine after extraction and in the stripping solution after stripping. Extraction conditions: 2 mol L^{-1} 2-butyloctan-1-ol in kerosene, pH=7.5, O/A=4 and 25 °C. Stripping conditions: 0.1 mol L^{-1} NaOH, O/A=4 and 25 °C.

	Boron concentration (mg L^{-1})	
Time (min)	Extraction	Stripping
0	507.6	0
5	274.1	244
10	274.1	244
15	274.1	244
30	274.1	244
45	274.1	244
60	274.1	244

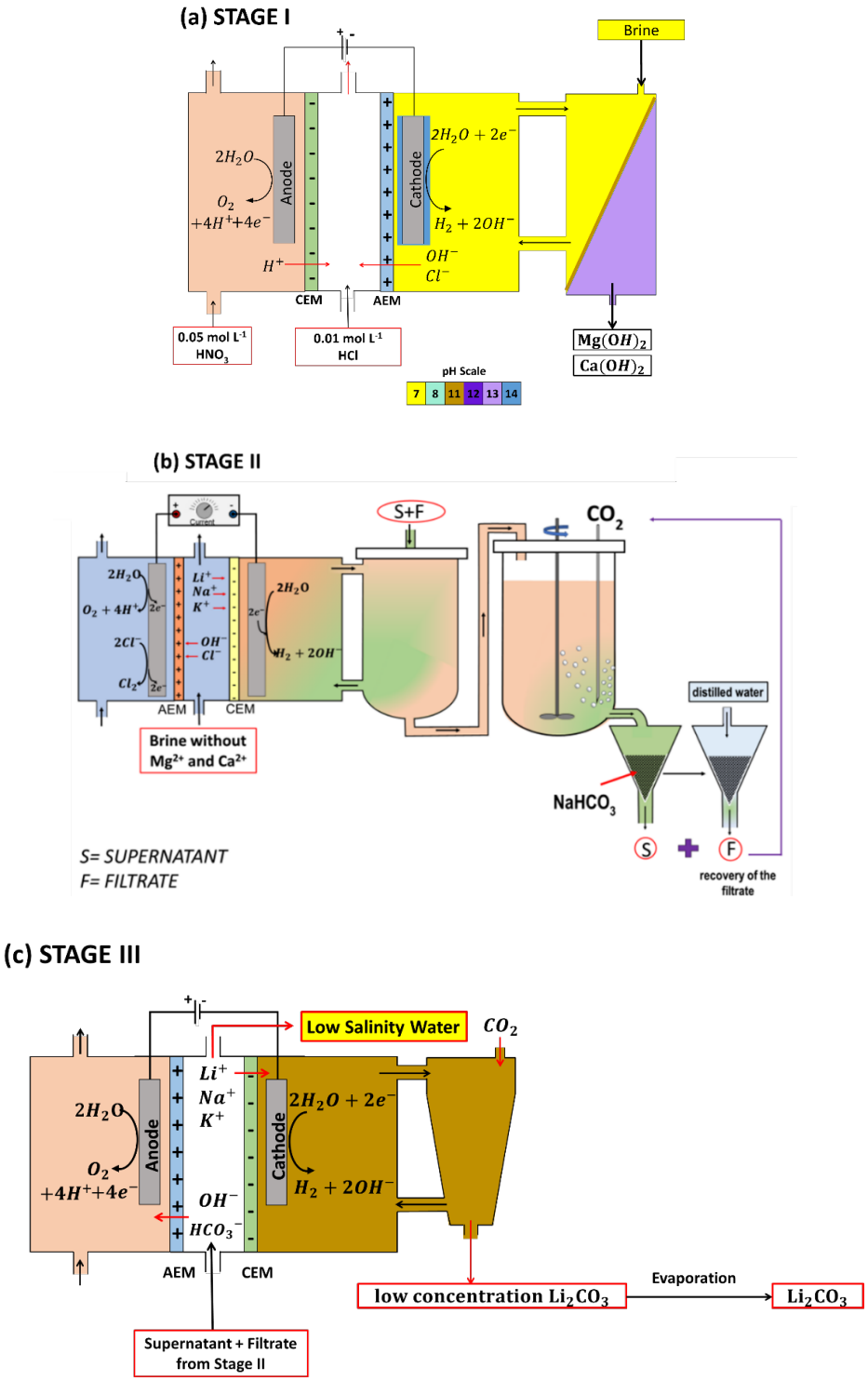

Figure A. 2: (a) Stage I, (b) Stage II and (c) Stage III implemented during the electrodialysis experiments.

Table A. 2: Technical specifications of ion exchange membranes. Data provided by the manufacturer (Membranes International Inc., https://ionexchangemembranes.com/).

Specification	AMI-7001CR	CMI-7000S
Functional group	Quaternary Ammonium	Sulphonic acid
Standard Thickness	0.450 ± 0.025	0.450 ± 0.025
Electrical Resistance (Ohm.cm^2) 0.5 mol/L NaCl	< 40	< 30
Maximum Current Density (Ampere/m^2)	< 500	< 500
Permselectivity (%) 0.1 mol KCl/kg / 0.5 mol KCl/kg	90	94
Total Exchange Capacity (meq/g)	1.3 ± 0.1	1.6 ± 0.1
Water Permeability (ml/hr/ft^2) @5psi	< 3	< 3
Thermal Stability (°C)	90	90

Table A. 3: Boron extraction efficiencies from the salar de Hombre Muerto brine as a function of the extraction step. Extraction conditions: 2 mol L^{-1} 2-butyloctan-1-ol in kerosene, pH=7.5, O/A=4 and 25 °C.

Extraction step	Extraction efficiency of boron (%)
1	46
2	64
3	68
4	70
5	76
6	80
7	82
8	90

Table A. 4: Evolution of pH, current, voltage, and concentrations of boron, calcium and magnesium in the non-pretreated brine in the cathodic compartment during the electrodialysis in stage I.

	Non-pretreated brine					
Electrodialysis time (min)	pH	[B] (mg L^{-1})	Current (A)	Voltage (V)	[Ca] (mg L^{-1})	[Mg] (mg L^{-1})
0	7.5	507.6	2.15	16.7	119.1	2315.9
60	8.7	487.3	2.15	7.3	91.6	1693.9
120	9.1	406.1	2.15	6.6	91.6	888.6
140	9.3	406.1	2.15	6.4	91.6	610.9
160	9.4	385.8	2.15	6.3	91.6	444.3
180	9.6	385.8	2.15	6.2	68.7	180.5
200	10.5	446.7	2.15	6.2	45.8	0.0
250	12.1	446.7	2.15	6	36.6	0.0
300	13.0	446.7	2.15	5.8	36.6	0.0

Table A. 5: Evolution of pH, current, voltage, and concentrations of boron, calcium and magnesium in the boron-depleted brine in the cathodic compartment during the electrodialysis in stage I.

	Boron-depleted brine					
Electrodialysis time (min)	pH	[B] (mg L^{-1})	Current (A)	Voltage (V)	[Ca] (mg L^{-1})	[Mg] (mg L^{-1})
0	8.8	50.8	2.15	16.7	91.6	2054.9
33	9.4	50.8	2.15	8.2	91.6	1555.1
70	9.6	50.8	2.15	7.1	91.6	1055.2
107	9.7	50.8	2.15	6.8	68.7	624.8
143	9.9	50.8	2.15	6.4	45.8	194.4
180	11.8	50.8	2.15	6.3	22.9	0.0
204	12.0	50.8	2.15	6.2	15.3	0.0
233	12.1	50.8	2.15	6.2	3.7	0.0
260	12.2	50.8	2.15	6.1	3.7	0.0
284	12.3	50.8	2.15	6.1	0	0
300	12.4	50.8	2.15	6	0	0

Table A. 6: Solubility of the salts (hydroxides and carbonates) in pure water (* solubility at 20 °C, solubility at 25 °C×) [28]. As the literature provides few data of solubility values in the brines mentioned in this paper, the values of salts solubility in water was taken as a reference.

Compound	Solubility (g L^{-1})
KOH	1,207.5×
NaOH	1,000×
LiOH	124.9×
$Ca(OH)_2$	1.2*
$Mg(OH)_2$	6.9×10^{-3}*
K_2CO_3	1114.2
$KHCO_3$	362.4
Na_2CO_3	307.2
$NaHCO_3$	102.8
Li_2CO_3	13.0

Table A. 7: Composition of the solid obtained for (1) the non-pretreated brine and (2) the boron-depleted brine after magnesium and calcium precipitations in stage I of the electrodialysis process.

	Mass fraction (%)							
Solid	B	K	Li	**Mg**	**Na**	**Ca**	**Cl^-**	SO_4^{2-}
(1)	0.3	1.7	0.2	5.6	28.8	0.4	44.6	3.8
(2)	0.2	1.6	0.2	6.9	28.8	0.4	43.9	3.9

Table A. 8: Values of pH in the three compartments, current, voltage, and concentrations of sodium, lithium and potassium in the middle compartment at the end of each electrodialysis experiment in stage II for the boron-depleted brine.

Experiment	Time (min)	pH of brine	pH anolyte	pH of catholyte	Na (mg L^{-1})	Li (mg L^{-1})	K (mg L^{-1})	Current (A)	Voltage (V)
0	0	12.4	11.4	9.4	89315	560	7427.5	0.75	3.9
1	2110	13.0	8.1	13.4	74820	629.5	3394	0.75	3.9
2	4394	13.5	11.6	13.6	43441	517.6	898.5	0.75	3.9
3	5461	11.8	12.8	13.6	251	6.8	0	0	30

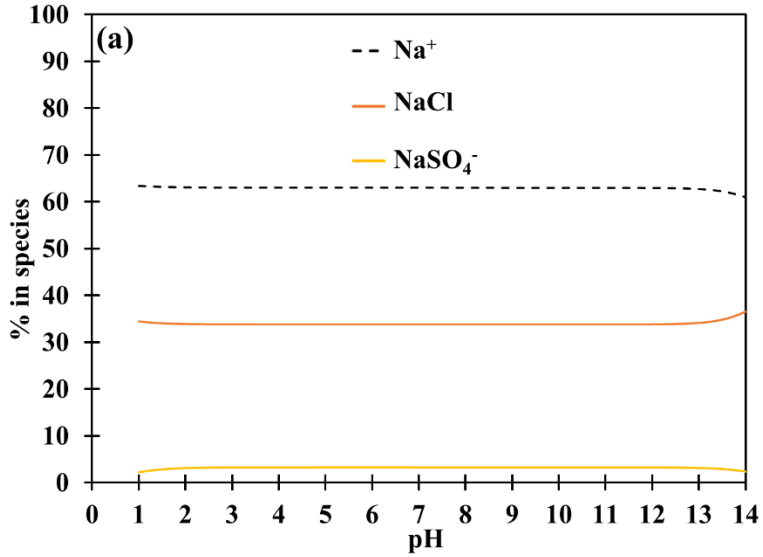
(a)
Na+
NaCl
NaSO4-
% in species
pH

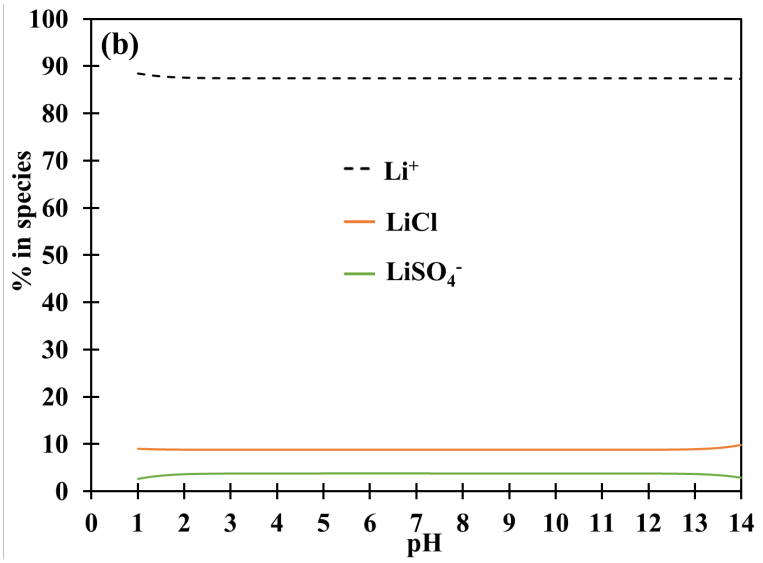
(b)
Li+
LiCl
LiSO4-
% in species
pH

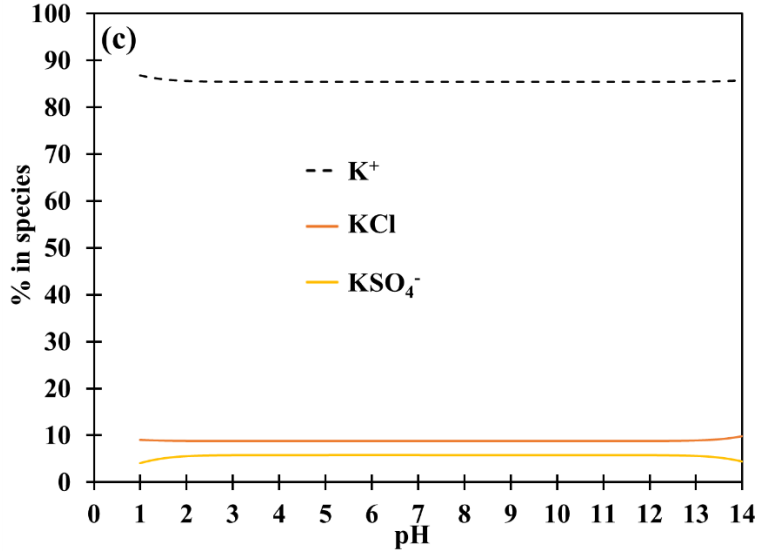
(c)
K+
KCl
KSO4-
% in species
pH

Figure A. 3: Speciation of (a) sodium, (b) lithium and (c) potassium vs pH in the boron-depleted brine before stage II of the electrodialysis process.

Aknowledgements

*T*his work was supported by the french PIA project "Lorraine Université d'Excellence", reference ANR-15-IDEX-04-LUE *and the LabEx RESSOURCES 21 through the national program "Investissements d'ave- nir" with the reference ANR-10-LABX-21-RESSOURCES21*.